MATERIALS SCIENCE AND ENGINEERING

Director's R&D Fund

Quantum Drops: Synthesis and Spectroscopy of a New Class of Luminescent Polymer Nanoparticles

M. D. Barnes,[1] B. G. Sumpter,[1] D. W. Noid,[1] and T. G. Thundat[2]
[1]*Chemical Sciences Division*
[2]*Life Sciences Division*

The primary aim of this project was to develop instrumentation and methodology for production and spectroscopic characterization of polymer-based quantum dots or quantum "*drops*." Proof-of-concept demonstration would enable development of a new class of luminescent nanoscale materials with tunable properties that could provide on-demand production capability without specialized synthetic hardware or toxic materials. Our overarching goal was to develop new materials and techniques for nanoscale optical (photonics) applications. To this end, ultrasensitive instrumentation for size-correlated optical imaging and spectrographic analysis was developed. To our knowledge, this instrumentation is unique at ORNL, and one of only a few with similar capabilities in the world. In addition to probing polymer quantum particles, we also examined luminescence from single ions in rare-earth doped nanocrystals and developed techniques for creating three-dimensional (3-D) artificial molecules from polymer-blend particles.

Introduction

Our LDRD program began by probing quantum-confined electronic states on the surface of polymer nanoparticles, which we call quantum drops. From this original proposal idea, we have explored a slightly different direction where we are using semiconducting polymers for quantum dot applications as "soft-material" analogues of inorganic semiconductor quantum dots. In contrast with conventional inorganic semiconductor nanoparticles, these species are prepared directly (and on demand) from bulk-material in solution in a few minutes, and no toxic materials (e.g., arsenic or selenium) or specialized synthetic procedures (other than the bulk material synthesis) are required. In addition we have recently discovered a new material of nanoscale and microscale polymer-blend spherical particles which allows formation of robust 3-D structures with a programmable architecture and tunable optical coupling. We call these species "photonic polymers" where the monomer units are the individual polymer particles. Finally, we have examined spectroscopic properties of semiconducting polymer nanoparticles. Preliminary results indicate that luminescent polymer nanoparticles can be formed in a crystalline state with a rod-shaped morphology. We have also observed that these rod-shaped particles can be oriented in a weak electrostatic field, suggesting the possibility of nanoscale optoelectronic polymer-based devices with applications to molecular computing, optical information encoding, photonic sensors, or advanced display technologies.

Technical Approach

Our experimental approach is based on liquid droplet techniques to produce nanoscale polymer particles of essentially arbitrary size. This has the advantage of on-demand generation of nanoscale species without specialized chemical synthesis; dots of a particular material are prepared through solutions of arbitrary bulk-phase materials. In order to correlate optical or spectral properties with particle size, we have designed and built an integrated atomic force microscope and high numerical aperture optical imaging system. The spectral properties of individual polymer dots were explored using techniques similar to single-molecule spectroscopy where single nanoparticles are illuminated and imaged with either a high-speed camera or a spectrograph.

Our first goal was to investigate the spectroscopy of charged polymer nanoparticles whose excess electrons (or holes) were predicted to have localized states[1] similar to metal—or semiconductor clusters.[2] The proof-of-concept idea was to use laser-induced fluorescence techniques to probe artificial atom resonances in charged nanoparticles. A significant complication in this effort was the lack of theoretical predictions of transition frequencies and oscillator strengths for these species. While we were able to obtain a Hartree-Fock level description of the electronic structure for surface-bound excess electrons on a 5-nm polymer sphere,[3] our limited budget precluded detailed theoretical analysis that would have enabled predictive spectroscopic information. Experimentally, the

search for quantum effects in polymer nanoparticles is complicated by effects of size and morphological dispersity that would tend to obscure sharp spectroscopic features in an ensemble measurement.

Our approach was to dope the nanoscopic polymer particles with fluorescent dye, which would in turn, act as a broad-band near-field excitation source for surface-bound electrons. By isolating individual particles on a glass coverslip, we were able to probe for artificial atom resonances without the necessity for wavelength scanning and without effects of ensemble averaging. To do this required a method for size characterization of individual particles with nanometer-scale resolution. We used a modified Digital Instruments Bioscope atomic force microscope that was integrated on a Nikon TE300 inverted microscope. Position registration between the cantilever and optical imaging worlds was achieved by using a thin (0.002 in.) laser-drilled pinhole (2-μm diam.) mounted on a glass coverslip. With the laser beam axis fixed, the pinhole was centered on the laser beam axis by noting the symmetry of the Airy diffraction pattern of the transmitted laser beam. Then the cantilever was engaged to scan the surface of the pinhole, providing a position reference between atomic force microscopy (AFM) and optical imaging coordinates. Optical resonances were probed by doping the particle with fluorescent dye, which was excited by a fixed-wavelength argon ion laser. Our expectation was that, by measuring the emission spectrum of an isolated particle, we would find artificial atom (quantum dot-like) transitions superimposed on the fluorescence spectrum of the dopant dye.

Results and Accomplishments

Using fluorescent dye as a broad-band excitation source of artificial atom resonances produced limited success. The major drawback was dye photostability; the signals were strongest near the peak of the dye emission profile, and resonance signals were obviously limited by photobleaching of the dye. Both of these factors combined to make the search for such resonances very difficult. Nevertheless, some interesting spectral features were observed from dye-doped nanoscopic particles, which we tentatively interpreted as originating from optical transitions of excess electrons. In particular, we observed interesting band structure superimposed on the continuum emission from the fluorescent dye for liquid-crystal polymer nanoparticles. These types of polymers are of interest because of the possibility of forming rod-shaped nanocrystalline phases[4] which would result in directional light output.

To address issues of photostabilty and tunable morphology, we investigated use of semiconducting polymers for quantum dot applications as "soft-material" analogues of inorganic semi-conductor quantum dots. In collaboration with Professor Mark Dadmun in the Chemistry Department at The University of Tennessee, we have synthesized a semiconducting polymer (a polyphenylene-vinylene derivative known as MEH-PPV), with a bulk bandgap of about 2 eV corresponding to orange-yellow (bulk) luminescence. We observe blue-shifted emission from nanoscale particles in the size range of 5–10 nm, suggesting the existence of quantum-confined excitonic states in these polymeric materials. However, as indicated by polarization analysis, the nature of these quantum-confined states for polymeric nanoparticles is quite different in polymeric particles in that the excitonic transition moment is highly oriented (near 100% extinction of the luminescence under orthogonal polarization). This suggests that the polymer molecules coalesce into rod-shaped structures upon droplet evaporation. In contrast with conventional II-VI inorganic semiconducting nanoparticles, these species are prepared directly (and on demand) from bulk material in solution in a few minutes, and no toxic materials (e.g., arsenic or selenium) or synthetic procedures are required. These results suggest the possibility of nanoscale optoelectronic polymer-based devices with applications to molecular computing, photonic sensors, or advanced display technologies.

In collaboration with Professor Rob Dickson at Georgia Tech., we used emission pattern imaging techniques to probe optically the morphology and orientation of MEH-PPV nanoparticles adsorbed on a glass coverslip. While there is extensive literature on these materials in micro-scale optoelectronic devices and thin-film applications, to our knowledge our study represents the first investigation of optical properties of isolated nanoparticles of a semiconducting polymer. Figure 1 shows an example of the optical emission pattern imaging data. For particles in the size range of 3–15 nm, we found a high degree of structural organization, providing evidence of a nanocrystalline phase in these small particles. Moreover, when the particles were produced with an excess (negative) charge, we found them to be oriented perpendicular to the coverglass substrate. Neutral particles were observed to be oriented in the plane parallel to the coverslip and showed significantly poorer photostability than the z-oriented nanoparticles. In-plane-oriented particles typically bleached within a few seconds, while z-oriented particles were stable for several minutes.

Figure 2 shows a closer look at the AFM data of the z-oriented MEH-PPV nanoparticles. The upper two panels are tapping-mode AFM surface scans of the same region of a glass surface with adsorbed MEH-PPV nanoparticles at two different contact forces. At low contact force (high setpoint), we observed a blurring of the particle image along the direction of the scan angle. At higher contact force, the lateral resolution became tip-radius limited (≈20 nm). For low contact-force imaging, the tip interacts

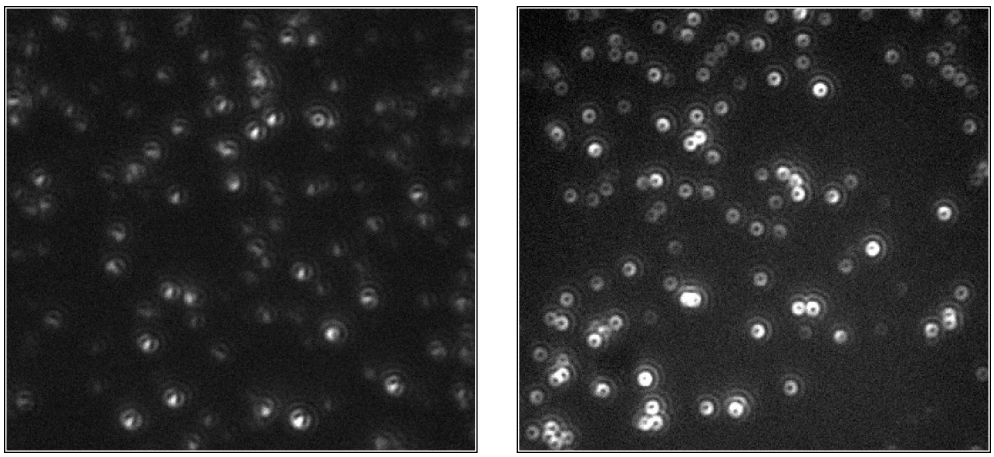

Fig. 1. Comparison of emission patterns from DiI(18) (a single chromophore molecule) spun coat in a polymethyl methacrylate thin film (left), and emission patterns from MEH-PPV nanoparticles (right) adsorbed on a clean glass surface. AFM surface height imaging indicated a narrow particle size distribution peaked at 5.5 nm. The observation of dipolar emission patterns for the MEH-PPV nanoparticles show that the chains are highly organized within the particles, and the "donut"-like emission patterns seen show that the stiff-chain segments are all uniformly oriented in the z-direction.

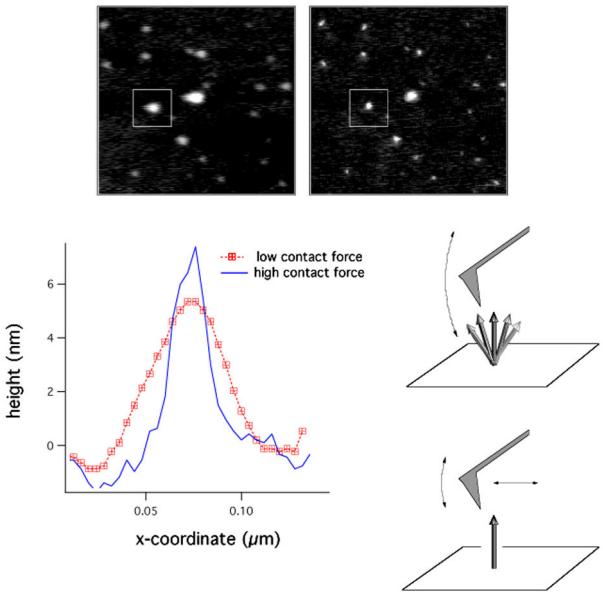

Fig. 2. Upper left and right: AFM surface scans in tapping mode of the same sample region with lower and higher contact forces, respectively. The lower left panel illustrates the broadening along the direction of the cantilever scan angle for the low (red markers) vs high (solid blue line) contact force scan for the particle indicated in the white square. The lower right panel shows a schematic of the tip-nanoparticle interaction at different imaging forces. At low contact force (high setpoint), the cantilever interacts with the particle near the turning point of its oscillatory motion, revealing an attractive particle-cantilever tip interaction that results in lever-like motion of the nanorod. This interaction appears as a lateral broadening in the surface height image. Conversely, in high contact force imaging, the tip encounters the particle with higher kinetic energy, thus suppressing the inelastic tip-particle interaction, and a tip radius-limited height image is observed. This effect would not be seen for a globular-like structure.

with the particle near the turning point of its oscillatory motion; the relatively low tip kinetic energy reveals an attractive interaction with the particle resulting in lever-like particle motion along the direction of the scan angle. At higher contact forces, the tip encounters the particle with higher kinetic energy, thus suppressing the tip-particle interaction. For a spherical globular structure, such a difference in surface height image with respect to contact force would not be observed. We have investigated techniques to improve photostability by preparing spherically or cylindrically symmetrical phase-separated structures where the PPV chromophores are insulated with a layer of low-molecular-weight polystyrene or other similar material. Preliminary experiments on polystyrene-MEH-PPV nanoparticles showed that the photostability of the PPV chromophore is significantly enhanced (≈20 ×) relative to the bare MEH-PPV, *without* affecting the phase-structure.

We pursued a related research direction designed to fabricate "molecular"-like structures from polymer particles. Using the same particle generation techniques, we have discovered a way to form 3-D linear or branched chains of polymer-blend microspheres generated from liquid droplets of solution. The modified surface structure of the polymer blend microspheres results in significant surface interpenetration to form highly robust particle-particle bonds. Using a linear quadrupole to manipulate the particles in space, we are able to take advantage of this novel material property to actively assemble particles in programmable 3-D architectures. The robust interlocking nature of interparticle linkage gives rise to strongly coupled morphology-dependent resonances, suggesting the possibility of nanoscale and microscale optical manipulation applications.

Summary and Conclusions

Our overarching goal was to develop new materials and techniques for nanoscale optical (photonics) applications. To this end, ultrasenstive instrumentation for size-correlated optical imaging and spectrographic analysis was developed. To our knowledge, this instrumentation is unique at ORNL and one of only a few with similar capabilities in the world. The work performed under LDRD support described here has resulted in 8 publications in peer-reviewed journals and 12 invited or contributed talks at universities and national meetings. We believe there will be several more publications to follow.

We are currently exploring several possibilities for follow-on funding including a collaborative proposal with The University of Tennessee to the Petroleum Research Fund to explore device applications of oriented polymer nanorods, and we are developing a full proposal in response to the DOE Office of Science Basic Energy Sciences Nanoscale Science and Engineering call for early in 2002.

References

[1]K. Runge, B. G. Sumpter, D. W. Noid, and M. D. Barnes, *J. Chem. Phys*. 110, 594 (1999).

[2]E. C. Honea, M. L. Homer, P. Labastie, and R. L. Whetten et al., *Phys Rev. Lett* **63**, 394(1989).

[3]S. Gray, B. G. Sumpter, M. D. Barnes, and D. W. Noid, *Chem. Phys. Lett.* **333**, 308 (2001).

[4]D. Hu, J. Wu, K. Wong, B. Bagchi, P. J. Rossky, and P. F. Barbara, *Nature* **405**,1030 (2000).

Publications Derived from This Project

A. Bartko, L. Peyser, R. M. Dickson, P. Kumar, M. Dadmun, A. Mehta, S. Mahurin, B. G. Sumpter, D. W. Noid, and M. D. Barnes, "Oriented Polymer Nanorods: Evidence for a nanocrystalline phase of a semiconducting polymer," to be submitted to *Nature*.

A. Bartko, L. Peyser, R. M. Dickson, A. Mehta, R. N. Bhargava, and M. D. Barnes, "Observation of dipolar emission patterns from isolated Eu^{3+}:Y_2O_3 nanocrystals," *Chemical Physics Letters* (submitted 9/24/01).

S. Mahurin, A. Mehta, B. Hathorn, K. Runge, B. G. Sumpter, D. W. Noid, and M. D. Barnes, "Photonic polymers: A new class of photonic wire structure from intersecting polymer-blend microspheres," *Optics Letters* (submitted 9/7/01).

M. D. Barnes, S. Mahurin, A. Mehta, B. G. Sumpter, and D. W. Noid, "Three-dimensional photonic molecules from sequentially linked polymer-blend microspheres," *Physical Review Letters*, in press (accepted for publication 11/2/01).

S. K. Gray, B. G. Sumpter, D. W. Noid, and M. D. Barnes, "Quantum mechanical model of localized electrons on the surface of polymer nanospheres," *Chemical Physics Letters* **333**, 308–313 (2001).

M. D. Barnes, J. V. Ford, B. G. Sumpter, D. W. Noid, and J. U. Otaigbe, "Nanoscale optical probes of polymer dynamics in ultrasmall volumes," published in *Computational Studies, Nanotechnology, and Solution Thermodynamics of Polymer Systems*, Kluwer Academic/Plenum Publishers, New York (2000).

K. Fukui, B. G. Sumpter, M. D. Barnes, and D. W. Noid, "Atomistic Dynamics of Nanoscale Polymer Particles," *Macromolecules* **33**, 5982–5987 (2000).

M. D. Barnes, A. Mehta, T. G. Thundat, R. N. Bhargava, V. Chhabra, and B. Kulkarni "On-off blinking and multiple bright states of single europium ions in Eu^{3+}:Y_2O_3 nanocrystals," *Journal of Physical Chemistry* B **104**, 6099–6102 (2000).

Carbon Nanotube–Based Molecular Electronic Devices

D. B. Geohegan,[1] M. L. Simpson,[2] P. F. Britt,[3] D. C. Joy,[4] S. J. Pennycook,[1] D. H. Lowndes,[1]
A. A. Puretzky,[5] X. Fan, M. A. Guillorn,[2] and D. W. Austin[2]
[1]*Solid State Division*
[2]*Engineering Science and Technology Division*
[3]*Chemical Sciences Division*
[4]*Metals and Ceramics Division*
[5]*Department of Materials Science and Engineering, The University of Tennessee*

The purpose of this project was to help meet ORNL's need for an interdisciplinary program in carbon nanotubes (CNTs) for molecular electronic devices. The project involved acquiring fundamental knowledge and simultaneously developing new techniques in four areas: carbon nanotube synthesis, characterization, chemistry, and electronic device development. First, time-resolved in situ diagnostics were applied to understand and control single-wall carbon nanotube growth. The mechanism by which carbon nanotubes grow was elucidated, and synthesis conditions were adjusted to provide carbon nanotubes that were easier to purify by chemical treatments. Raman spectroscopy, field-emission scanning electron microscopy (FESEM), transmission electron microscopy (TEM), and electron energy-loss spectroscopy techniques (EELS) were developed to characterize CNT purity and structure. Chemical techniques were developed to purify CNTs and functionalize the nanotubes for their assembly in prototype electronic devices. Lithographic microfabrication techniques were developed to position CNTs into prototype electronic devices, and fundamental electronic measurements were made to understand charge transport in CNTs. The project met its goals to achieve international recognition in each of these areas and derive fundamental knowledge and specialized techniques to sustain further program development in CNT–based electronic devices.

Introduction

Single-walled carbon nanotubes (SWNTs) have electrical properties which are directly determined by their atomic structure. In the 10 years since SWNTs were discovered, research on their electronic properties and chemical functionalization has provided strong evidence that SWNTs (in striking contrast to earlier fullerenes) will enable major advances in nanoscale electronic devices, microelectromechanical systems (MEMS), biological probes, and field emission devices. Possibly of greatest significance, CNTs may provide the means for molecular interconnection and for input/output (I/O) between the macro- and nano-domains that will allow the realization of molecular-scale computing devices. Recent experiments also show that SWNTs are highly thermally conductive, resistant to high temperatures and harsh chemicals, lightweight, incredibly strong in the axial direction (1-TPa Young's modulus) and resilient in the transverse, and their hollow structure makes them ideal for hydrogen storage and drug delivery. These properties broaden the scope of CNT applications into aerospace, transportation, and biotechnology, making them extremely attractive commercially and vitally important to national energy, economic, security, and defense goals.

At the beginning of this project, many research groups in the world had developed carbon nanotube programs incorporating one or two components of synthesis, characterization, chemistry, and electronic measurement techniques for device development. Similar fractionated efforts existed at ORNL. However, three grand challenges in nanoscience obstructed the development of carbon nanotube–based electronic devices. First, the fundamental mechanisms of carbon nanotube growth were not understood, so their electronic properties could not be controlled during synthesis. Second, carbon nanotube chemistry was poorly characterized, so methods of purification, solubilization, and functionalization of carbon nanotubes for optimized device properties were not developed. In addition since carbon nanotube chemistry strongly depends on the structure and extent of defects introduced during the synthesis process, unlinked synthesis and chemistry efforts provide no mechanisms for understanding nanotube chemistry. Third, fundamental understanding of carbon nanotube electronic transport properties was seriously hampered by a lack of

understanding of their chemical sensitivity and other factors, such as contact resistance to metal electrode test structures. Again, the electronic properties of carbon nanotubes for devices could not possibly be understood without a coordinated program involving well-characterized synthesis, chemistry, and electronic measurements. This project addressed the Laboratory's need for just such a program and offered the mechanism by which ORNL could establish itself rapidly in a field with so much competition.

Technical Approach

A coordinated approach which interlinked SWNT synthesis, characterization, chemistry, and device assembly and electronic measurements was implemented. Unique in situ diagnostics were employed during nanotube synthesis to gain fundamental understanding of growth mechanisms and characterize the nanotube growth environment such that the exact growth conditions could be exactly repeated. The nanotubes produced in these experiments were then harvested and examined by a battery of characterization tools such as FESEM, TEM, EELS, and Raman spectroscopy to (a) relate fundamental properties (purity, length, bundle size) of the nanotubes to the growth environment (thereby determining growth rate, etc.) and (b) help understand subsequent chemical processing results. These nanotubes were then subjected to chemical processing treatments in order to purify and functionalize the nanotubes for use in electronic devices. Following chemical treatment, the nanotubes were again characterized prior to the measurement of their electronic properties. Finally, nanotube test structures were designed and fabricated, and the electronic transport through carbon nanotubes from the chemical treatments was measured.

This coordinated approach for the development of carbon nanotube electronic devices placed constraints on each task area. Carbon nanotubes could no longer be synthesized without regard for the difficulties in their purification. Chemical treatments for purification were required which would not damage the nanotubes' electronic properties. Characterization tools needed to be developed which were good indicators of these properties. Electronic properties measurements were also needed to overcome the challenges in sample preparation which were complicating similar efforts worldwide, while differentiating between the effects introduced by the team's synthesis and chemical processing.

SWNT synthesis was accomplished by laser vaporization of carbon targets which incorporated ~1 at % metal-catalyst powders (Ni,Co). Time-resolved, gated, intensified-CCD-array imaging of laser-induced fluorescence, incandescence, and Rayleigh-scattered light allowed tracking of the plume of vaporized material in 500-Torr argon gas as it traversed the tube furnace environment (700–1200°C oven temperatures). Compositional analysis of the plume was accomplished by gated spectroscopy with a gated, intensified diode array and spectrometer system.

The SWNT material was harvested from various locations inside and outside the oven and examined by characterization tools. TEM was used to observe the catalyst size and nanotube length, and FESEM was used to estimate bundle size and overall sample purity; however, thermogravimetric analysis (TGA) was the ultimate judge (see below). A microRaman spectroscopy setup was developed in this project for routine ex situ analysis of the materials and was capable of observing even minute fractions of SWNT .

Approximately 200-mg quantities of raw SWNT material was subjected to various chemical treatments to investigate methods for purification. Purification involves the removal of the metal catalyst particulates and the removal of amorphous carbon material that did not convert into nanotubes. Graphitic carbon was nearly impossible to remove and had to be avoided in the synthesis step. Methods developed included extended reflux in nitric acid (to remove the metal catalyst) and selective oxidation of the amorphous carbon (using the difference in burning temperature between amorphous and crystalline carbon). The selective oxidation temperature was determined by TGA for each raw material. The purification procedure was sensitive to the synthesis conditions, and these two steps were coordinated.

Purified SWNTs were provided in thick bundles congealed in solid mats. For electronic characterization, techniques needed to be developed to suspend the nanotubes in a solvent, break the bundles into individual SWNTs, and disperse the nanotubes across prepatterned test structures. Lithographically patterned test structures were designed and fabricated at the CNF (Cornell Nanofabrication Facility). Nanotubes were spun, sprayed, and dipped for random dispersal onto these test structures. Atomic force microscopy (AFM) and scanning tunneling microscopy (STM) were developed in this project to characterize single nanotube bundles on substrates. Methods were also developed to electrodeposit metal onto nanotubes near test leads to form good electrical contact. Methods were also developed to lithographically place metal electrodes on top of randomly dispersed nanotubes. Transport measurements [current-voltage (I-V) curves] were performed to characterize the nanotube properties. Electronic devices, such as field-effect transistors, were developed and demonstrated.

This entire procedure was iterated for different synthesis procedures. Throughout the program, an extremely interactive team approach was necessary, and the project served to supply SWNT for various programs and experiments within the laboratory.

Results and Accomplishments

Fundamental Measurements of Single-Wall Carbon Nanotube Synthesis Mechanisms were performed using time-resolved, in situ diagnostics of the plume of material vaporized from a carbon-metal catalyst target. The results are summarized in Fig. 1. These measurements revealed that SWNT grow from the conversion of condensed-phase carbon material by metal clusters and nanoparticles over extended times (up to several seconds) at growth rates between 1 and 5 μm/s. To confirm this supposition, short SWNT were synthesized by restricting the time available for growth to ~25 ms through the use of intensified CCD imaging and thermophoretic forces exerted by temperature gradients near the exit of the furnace. From the length of these SWNT, and a knowledge of the time spent at high temperature, the growth rates of SWNT inside the hot furnace environment were estimated for the first time. These SWNT were then subjected to rapid thermal annealing treatments, and growth from ~50-nm-long SWNT to microns in length was observed through careful analysis of length distributions measured before and after annealing. Growth was observed only in the 900–1300°C temperature range, very similar to that inside the hot oven during the laser vaporization process. These results support the theory that the growth mechanism during laser-vaporization production is a *condensed-phase conversion* process.

Resonant Raman Spectroscopy was developed as a key characterization tool in this project for the purity, diameter distribution, and distribution of metallic-vs-semiconducting SWNT in the samples. A high-throughput (f1.8 Holospec) spectrometer with CCD detector was coupled to an optical microscope to provide sensitive detection of SWNT within a ~5-μm region of the sample. An example of Raman spectra from both long and short SWNT is given in Fig. 2 (a,b) which shows the tangential modes which match the energy separation between one-dimensional (1-D) singularities in the 1st valence band and the 1st conduction band in metallic SWNTs, E_{11}^{M}. Both metallic and semiconducting nanotubes can be

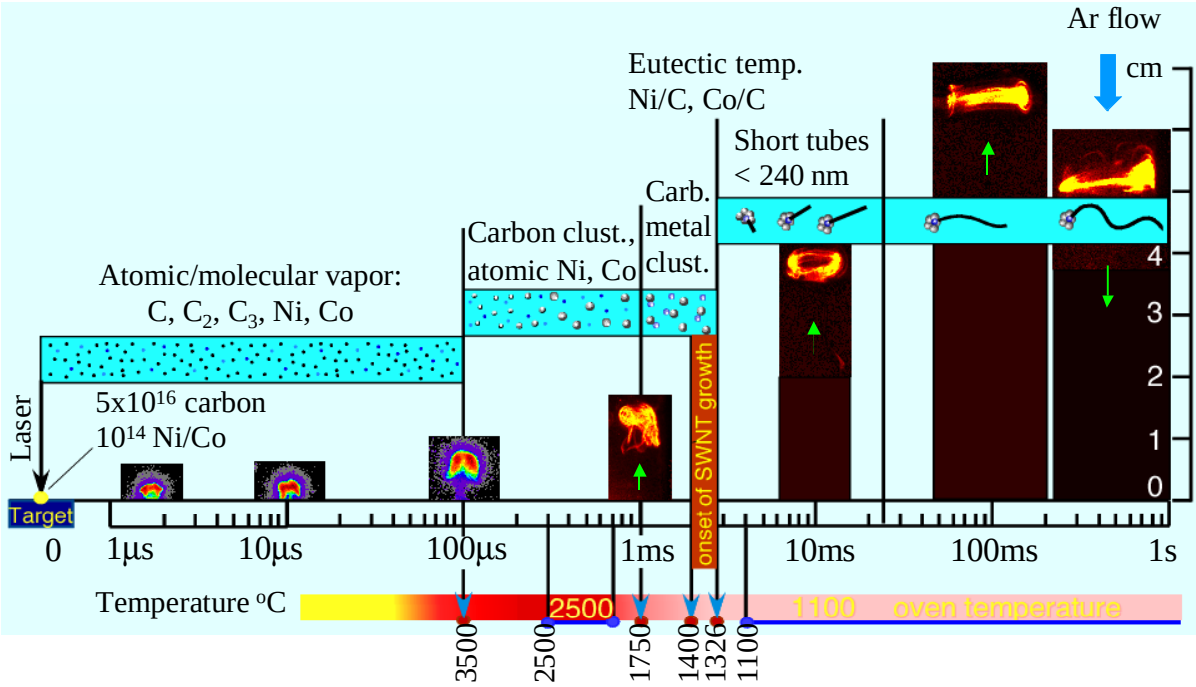

Fig. 1. A compendium of the results from the in situ imaging and spectroscopic diagnostic investigations of SWNT growth inside a hot oven. Actual images of the laser plasma (t <200 μs) and Rayleigh-scattering (RS) images of the plume (t >200 μs) are shown vs time (scale in cm at right). During the first 100 μs after ablation, the laser plasma is very hot, and emission from excited atoms and molecules dominate laser-induced fluorescence (LIF) from ground state species. Ground state populations then peak and subsequently disappear due to condensation. Images and LIF spectra show that carbon condenses by t = 200 μs after ablation, while the metal catalyst atoms condense much later. The ground-state atomic Co population is maximum at t = 1 ms, and then condenses by t = 2 ms. By t = 2 ms, no LIF is detectable, only laser-induced luminescence and RS from clusters and nanoparticles (i.e., nearly all atoms and molecules have converted into clusters and nanoparticles, as evidenced by the vortex ring structure of the plume). At t = 2 ms, the plume temperature is ~1400°C, just above the Ni/C and Co/C eutectic temperatures. By t = 4 ms, the plume has thermalized to the oven temperature. If growth is stopped at t ~25 ms, only short nanotubes are found (<240 nm in length), indicating that the majority of growth takes place over much longer times, during the ~10-s traversal time through the oven, past the target, to the collector. These results indicate that the majority of growth occurs from condensed clusters and nanoparticles of carbon and metal catalyst in contact with one another, a condensed-phase conversion *process.*

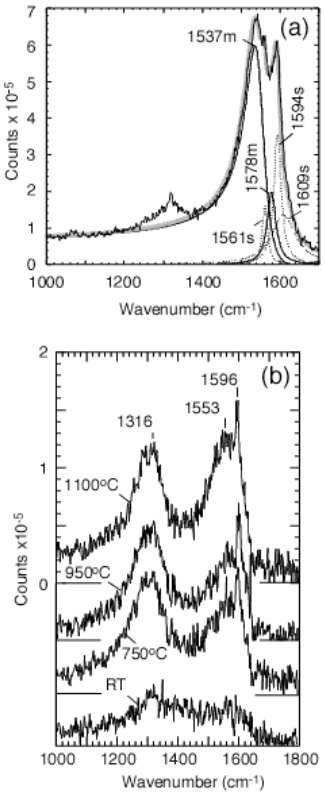

Fig. 2. Resonant Raman spectra (RRS) of SWNT produced by laser ablation, as observed by 632.8-nm (1.96-eV) excitation show the following: (a) the tangential modes of long nanotubes as produced for chemical purification (both metallic and semiconducting nanotubes can be observed) and (b) RRS of short (~50-nm-long) SWNT synthesized by restricting the growth time via in situ diagnostics at three indicated oven temperatures. The spectra shows that the short SWNT are well formed structurally but exhibit a defect band ~1316 cm^{-1} due to the ends of the nanotubes.

characterized with this technique. The main feature of the tangential band of the long SWNTs around 1537 cm^{-1} can be fitted with a Breit-Wigner-Fano (BWF) line shape. This feature is typical for metallic SWNTs and originated from the lower frequency A(A_{1g}) Raman component of the metallic tubes. The BWF line shape of this component is due to coupling of the discrete phonons to an electronic continuum. The higher frequency A(A_{1g}) metallic component around 1578 cm^{-1} is not coupled to the electronic continuum and has a Lorentzian line shape. The peak around 1594 cm^{-1} is related to semiconducting nanotubes. This feature is typical for semiconducting tubes and appears probably because of the laser resonance with the energy separation between 1-D singularities in the 3d valence and the 3d cataconduction bands, $E_{33}^{S}(d_t)$, for the larger tube diameters, d_t. The semiconducting tangential band can be fitted with three major components.

Figure 2b presents Raman spectra of short SWNTs such as those shown in Fig. 3. The short SWNTs exhibit the same main Raman peaks as the long tubes, which shows that they are well formed structurally. A new peak in the Raman spectra occurs, however, around 1316 cm^{-1}, which according to theory, arises from the finite length of the electronic structure of carbon nanotubes. As the length of the SWNT increases, the density of states spectrum of SWNTs changes from that characteristic of a zero-dimensional system to that typical of a 1-D system after

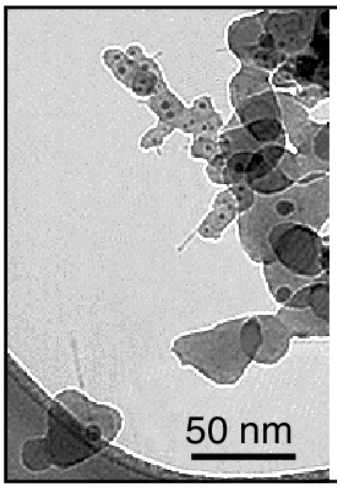

Fig. 3. TEM image of short SWNT grown by restricting the time spent by the ablation plume inside the hot oven using in situ diagnostics. Few short nanotubes <50 nm are shown. The nanotubes protrude from some of the many small (<20-nm diameter) black metal catalyst particles in the image. The majority of the material in the image is unconverted carbon. This material was subjected to annealing treatments to see if SWNT growth could be reinitiated.

SWNTs grow to about 10-nm lengths. In summary, we can characterize metallic and semiconducting SWNT, including those of very short length.

Purification of SWNT. Crude SWNTs were found to contain metal catalyst (1 at % Ni and Co ca. 9 wt %) and amorphous carbon. The metal catalyst was present as nanoparticles encased in a carbon shell that was relatively impervious to acid. After many attempts, a general protocol was established to screen and purify the crude SWNT samples. Crude SWNTs were refluxed in 3 *M* HNO_3 for 16 h, filtered (0.2 μm), and air oxidized at 550°C for 30 min. Additional acid treatment reduced the metal content to ≤0.3 at % (by EDX analysis on multiple spots). As the samples became purer, the size of the nanotube bundles increased (by FESEM analysis, see Fig. 4). Thermogravimetric analysis (TGA) in air was used to screen the samples and follow the purification process. It was found that as the metal content of the samples decreased, the temperature for maximum weight loss (DTG) increased from 400°C to 700°C. In general, DTG for the crude, acid-treated and air-oxidized samples showed transitions between 390°C and 410°C, 505°C and 565°C, and 690°C to 730°C, respectively (see Fig. 5). After acid treatment, two transitions were typically observed centered at 515°C and 560°C, but the relative intensity of these transitions did not correlate with the final yield of SWNT after purification. Although a high temperature peak, similar to the one reported by the researchers at NREL, was sometimes observed at 660°C to 680°C, this transition did not correlate with purified yields of SWNTs. Using the general purification procedure outlined above, the yield of purified SWNTs was 10.5 ± 1.4 wt %. One unresolved question that remains is the extent of damage caused by the chemical purification. Raman spectroscopy provides insight into this question, but additional characterization techniques are needed.

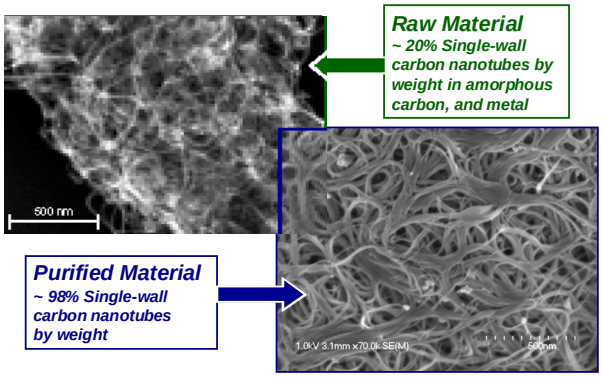

Fig. 4. FESEM images of "raw" SWNT ropes directly taken from the collector, and a mat of "purified" SWNT "buckypaper" after acid treatment, oxidation, and filtration to remove metal nanoparticles and amorphous carbon.

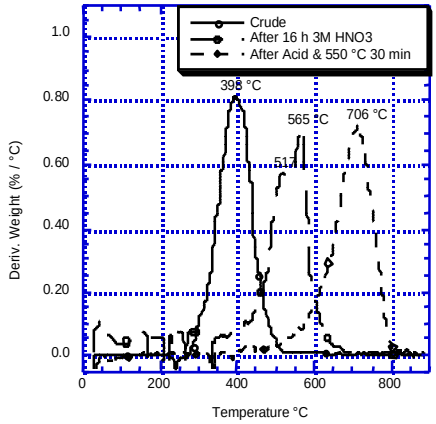

Fig. 5. DTG of SWNTs in air: crude, refluxed in 3 M HNO_3 for 16 h, and acid treated followed by heating to 550°C in air for 30 min.

Throughout the project, the laser ablation conditions were changed to maximize the yield of SWNTs, but this also altered the types of impurities and their ease of removal. For example, it was discovered that short laser pulses (8-ns full width at half maximum, 300 mJ) produced a lower yield of SWNTs that contained a higher metal content while long laser pulses (180-µs full width at half maximum, 300 mJ) produced a higher yields of SWNTs and a lower metal content. However, the residual metal appears to catalyze the oxidation of the SWNTs. Thus, the final yield of purified SWNTs depends on how the metal is dispersed in the samples and the thickness and chemical constitution of the carbon shell surrounding the metal particle.

Electronic Transport Measurements were carried out for both raw and purified SWNT which were deposited on a variety of electrode test structures, as described above. Individual nanotubes were obtained by sonicating nanotube mats in solvents such as dichloroethane, dimethylformamide, and methanol and dipping, spin-coating, or spraying the nanotubes onto lithographically prepatterned substrates. The electrical characteristics of the nanotubes were measured, and prototype devices were investigated. AFM measurement techniques were developed to repeatedly locate the nanotubes and measure the effects of the electronic transport measurements on them.

Figure 6 shows a prototype field-effect transistor structure where a single 1.3-nm-diam SWNT is deposited across two gold electrodes. I-V measurements showed that this nanotube is semiconducting, but with a large (1.7-MΩ) contact resistance. In order to overcome the dominant effects of the nanotube-electrode contact resistance, a new technique was developed to electrodeposit metals onto the nanotube/electrode junction. This technique resulted in a significant reduction in the electrode-nanotube contact resistance without the requirement of an imaging and mapping process after nanotube deposition. Furthermore, the thin film of gold was deposited only on the electrodes and did not perturb the semiconducting behavior of the SWNT. However, the I-V characteristics of the CNT field-effect transistor (CNTFET) were significantly altered, possibly due to the work function difference between the original electrode material and the electroplated material or a mechanical change in the electrode/nanotube junction. Figure 7 shows the I-V characteristics of the CNTFET device for different gate voltages.

Such prototype devices, which use a single SWNT as a transistor element, represent the future of carbon nanotube–based logic elements. The fundamental issues of electron transport in single-walled carbon nanotubes

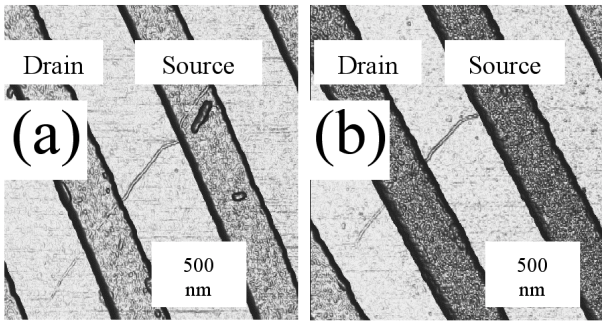

Fig. 6. (a) AFM image of a 1.3-nm-diam semiconducting SWNT deposited on two palladium electrodes. The prefabricated electrodes extend 36 nm above the substrate and are labeled as drain and source, respectively, indicating the configuration used for the charge transport measurements. (b) AFM image after electroplating gold onto the drain and source electrodes. The two center electrodes now extend 42 nm above the substrate, and the SWNT is buried under the electrodeposited layer of gold. The regions of the nanotube between the electrodes show no gold deposits. The gate for this field-effect transistor is a silicon wafer buried beneath the oxide layer on which the nanotube rests.

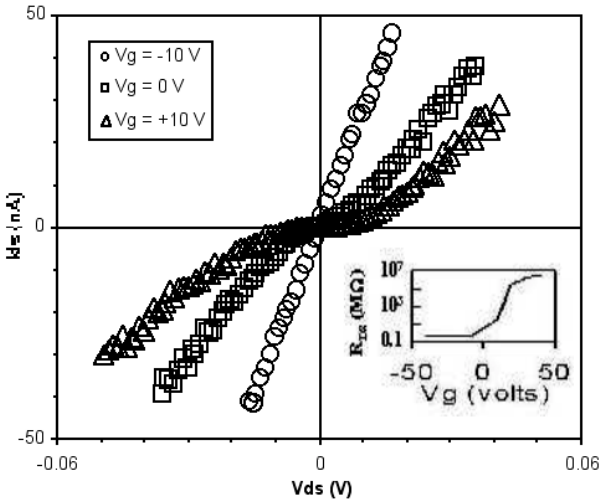

Fig. 7. Charge transport measurements for the field-effect transistor shown in Fig. 6(b). Electrodeposition of gold has decreased the contact resistance by a factor of 6. The inset shows that the low voltage resistance can be modulated over seven orders of magnitude by the gate voltage.

were addressed in this project, and the first prototype devices were developed as proposed in the original goals. Current research is focusing on the influence of mechanical deformation on the electronic properties of SWNT, a cross-cutting research direction which should impact the development of multifunctional nanotube composite materials which are strong, yet possess useful electronic properties.

Summary and Conclusions

This team has fulfilled its goal to establish the laboratory as an internationally recognized center for carbon nanotube research. Significant progress was made in fulfilling the goals and proof-of-principle experiments in each area of the program: (1) understanding and controlling the synthesis of SWNT, (2) new methods to characterize SWNT, (3) chemistry of carbon nanotubes, and (4) electronic device development and transport measurements. Significant new results are just reaching publication as a result of this project, and many more publications are in progress. However, the coordination and activity of the principals in this project—a direct result of the support and technical approach developed in this program—have already been recognized at international meetings with invited talks and symposium/session-chairing responsibilities at conferences, as well as invitations to speak at universities.

Key results of the project included determining the condensed-phase conversion mechanism (and rate) by which carbon nanotubes grow during laser-vaporization synthesis, development of coordinated synthesis and purification techniques capable of producing 98% pure SWNT, development of methods to disperse and contact individual SWNT on electrode test structures, and demonstration of molecular electronic devices (such as field effect transistors) using single SWNT.

This project has had immediate impact in bringing new funding to ORNL. New projects were funded with NASA-Marshall Space Flight Center for carbon nanotube thermal conductivity measurements, with NASA-Langley Research Center for the development of multifunctional nanotube composites, and with the Department of Energy for study of the condensed-phase growth of SWNT crystals. New opportunities for programs utilizing carbon nanotubes in biology, textiles, and structural materials have been enabled through the support of this project. Large proposals are pending with Defense Advanced Research Project Agency through their electronics and structural materials program managers.

This project has benefited the Laboratory in several ways. First and foremost, by tackling a project which has stymied the best research programs in the world, this project required the development of a team which relies upon one another, cutting across divisional boundaries. As described above, along with the technical accomplishments and journal publications, the success of this team approach has already been internationally recognized. However, more importantly, the support and collaborative spirit from this project has branched out to augment the research of many budding programs within ORNL and at The University of Tennessee. Since carbon nanotubes and the infrastructure necessary to study them are so central to so many projects in nanoscience today, this project served an essential role at a key time in the development of nanoscience at the Laboratory. The expertise developed in this project in carbon nanotube synthesis, characterization, chemistry, and electronics was recognized recently by the large regional agreement of a research focus area in carbon nanotubes at the planning workshop for the Center for Nanophase Materials Sciences. With this venue and the follow-on funding provided by the many outstanding proposals generated through this project, the Laboratory will continue to be a leader in the field of carbon nanotubes and their many applications.

Publications Derived from This Project

A. A. Puretzky et al., "In situ imaging and spectroscopy of single-wall carbon nanotube synthesis by laser vaporization," *Appl. Phys. Lett*. **76**, 182 (2000).

A. A. Puretzky et al., "Dynamics of single-wall carbon nanotube synthesis by laser vaporization," *Appl. Phys*. **A70**, 153 (2000).

D. B. Geohegan et al., "In situ plasma diagnostic investigations of single-wall carbon nanotube synthesis by laser ablation of C-Ni-Co targets," *Proceedings of the SPIE–The International Society for Optical Engineering*, 2000, vol. 3935, p. 2–13.

D. B. Geohegan et al., "Condensed phase growth of single-wall carbon nanotubes from laser annealed nanoparticulates," *Appl. Phys. Lett*. **78**, 3307 (2001).

A. A. Puretzky et al., "Time-Resolved Diagnostics of Single-Wall Carbon Nanotube Synthesis by Laser Vaporization," Proceedings of COLA'01, *Appl. Surf. Science* (submitted).

D. B. Geohegan et al., "Growth and Characterization of Short Single Wall Carbon Nanotubes by in Situ Diagnostics Controlled Laser Vaporization," *Appl. Phys*. (to be published).

D. B. Geohegan et al., "Laser Synthesis of Single Wall Carbon Nanotubes with Time-Resolved in situ Diagnostics," *Proceedings of the SPIE–The International Society for Optical Engineering*, 2001 (in preparation).

P. F. Briff et al., "Purification of SWNT prepared by Pulsed Laser Ablation" (in preparation).

X. Fan et al., "Nucleation of Single-Walled Carbon Nanotubes," in preparation (2001).

D. W. Austin et al., "Decreasing contact resistance between electrodes and single-walled carbon nanotubes by electrodeposition of Au," submitted to *Appl. Phys. Lett.*

V. I. Merkulov et al., "Alignment mechanism of carbon nanofibers produced by plasma-enhanced chemical-vapor deposition," *Appl. Phys. Lett*. **79**, 2970 (2001).

V. I. Merkulov et al., "Shaping carbon nanostructures by controlling the synthesis process," *Appl. Phys. Lett*. **79**, 1178 (2001).

M. A. Guillorn et al., "Fabrication of Gated Cathode Structures Using an In-Situ Grown Vertically Aligned Carbon Nanofiber as a Field Emission Element," *J. Vac. Sci. Tech.* **B19**, 573 (2001).

M. A. Guillorn et al., "Fabrication of Dissimilar Metal Electrodes with Nanometer Interelectrode Distance for Molecular Device Characterization," *J. Vac. Sci. Tech.* **B18**, 1177 (2000).

Designer Nanoscale Materials from Self-Assembly of Triblock Copolymers

G. D. Wignall,[1] A. Habenschuss,[2] and F. S. Bates[3]
[1]*Solid State Division*
[2]*Chemical Sciences Division*
[3]*University of Minnesota*

Block copolymers are molecules containing two or more chemically distinct polymers, each a linear series of identical monomers. In general, the components have different chemical affinities, and when they are incompatible, segregation occurs. The chemical bond between the blocks constrains the separation to length scales of the order of the block radius of gyration, thus producing complex nanostructures on length scales of 1–100 nm by self-assembly. Research has been undertaken to investigate many aspects of three-monomer (ABC) linear triblock copolymers, particularly those located near the order-disorder transition (ODT) where processing is feasible. Anionic polymerization was used to produce poly (isoprene-*b*-styrene-*b*-dimethylsiloxane) (ISD) and the analogue poly (styrene-*b*-isoprene-*b*-dimethylsiloxane) (SID). These polymers were characterized as a function of composition and temperature by techniques such as small-angle X-ray and neutron scattering (SAXS and SANS) and dynamic mechanical spectroscopy (DMS). Blends of ABC and ACB compounds and also the corresponding A, B, and C homopolymers were also studied. The limits of miscibility and the nanoscale morphologies encountered with blending were identified and compared with theory. The criteria for partial and complete disordering as a function of block sequencing was also established. Compositionally symmetric SID and ISD triblock copolymers with similar molecular weight (MW) disorder at different temperatures and display different pathways to disorder, different disordered-state properties, and full blend miscibility with a synergistic gyroid formation over a wide composition range. Relative magnitudes of the three different Flory-Huggins interaction parameters for this ABC system allow a detailed interpretation of SAXS, SANS, and DMS measurements. Symmetric SID disorders from the lamellar state, while ISD disorders from a morphology with hexagonally packed cylinders of D blocks in a matrix of mixed S and I block segments. We also explored the possibility of manipulating the morphology of triblock copolymers by adding controlled amounts of the corresponding homopolymers. In particular, we studied symmetric SID copolymers (volume fractions of S/I/D, 0.20/0.59/0.21) and equal volume fractions of polystyrene (PS) and poly-dimethylsiloxane (PDMS). When the total homopolymer volume fraction φ exceeds 65%, the blend macroscopically separates into ordered homopolymer-poor and -rich regions. Between $45\% < \varphi < 65\%$ homopolymer volume fraction, hexagonally packed core-shell cylinders form with PDMS cores and PI shells. Between 15% and 45% homopolymer volume fraction, a core-shell gyroid morphology is observed with PDMS cores and PI shells. These core-shell variations of the classical structures of diblock copolymers are attributed to a small asymmetry in segment-segment interaction parameters. The neat SID block copolymer has a new complex ordered microstructure.

Introduction

Block copolymers are macromolecules composed of long series (i.e., blocks) of chemically distinct repeat units (segments). The simplest molecular architecture is obtained by connecting a block of A units end to end with a block of B units to make an A-B diblock copolymer. More complex molecules can be created by linking together two or more diblock copolymers, or by synthesizing architectures based on two, three, or more monomer types (e.g., ABA or ABC triblock copolymers, etc.).

Two competing effects govern the thermo-dynamics. At high temperatures, the chains are mixed homogeneously as in a polymer melt. As the temperature is reduced, incompatible blocks tend to segregate due to the different chemical affinities of the components. The bond between blocks constrains intrachain separation to a length scale on the order of the overall chain radius of gyration.

All these materials have a common feature: *ordered structures with characteristic length scales between 1 and 100 nm*. These self-associating amphiphilic molecules have found applications in a wide range of industrial products such as polyurethane foam, used in upholstery and bedding, and box tape. The addition of block-copolymers to commodity plastics can enhance toughness or modify the surface properties and the ability to

independently specify the molecular architecture, composition, and the overall block sizes, providing an opportunity to manipulate the ultimate phase behavior of these materials.

Technical Approach

The nanostructure of an AB diblock copolymer is controlled by three variables: the overall degree of polymerization ($N = N_A + N_B$), the fractional composition ($f = N_A/N$), and the Flory-Huggins (FH) segment-segment interaction parameter (χ_{AB}). Adding a third distinct block introduces the following complications: The number of χ parameters triples (i.e., χ_{AB}, χ_{BC}, χ_{AC}), the number of composition variables doubles (i.e., f_A and f_B), and three distinct block sequences become possible (i.e., ABC, ACB, and CAB). There are four equilibrium diblock morphologies: spheres, cylinders, lamellae, and the gyroid. Assuming the number of phases is governed by a simple combinatorial relationship, then linear ABC triblock copolymers would be anticipated to exhibit hundreds of distinct morphologies, though to date only 20 have been identified.

One method of manipulating the morphology of a three-monomer block copolymer, while avoiding the complexities described above, is to add judicious amounts of the corresponding homopolymers, and this strategy is exploited in many products prepared from AB and ABA block copolymers. Because to date few studies have been performed along these lines, the aim of this project was to explore the morphologies found in linear ABC triblock copolymers and how to manipulate them by adding the corresponding A, B, and/or C homopolymers. We used SANS, SAXS, and microscopy to provide structural insight into the various morphologies probed.

Results and Accomplishments

The SID and ISD triblock copolymers discussed in this report were prepared using anionic polymerization techniques; volume fractions were calculated based on the published homopolymer densities at 140°C for each block ($\rho_S = 0.97 g/cm^3$, $\rho_I = 0.83\ g/cm^3$, $\rho_D = 0.89\ g/cm^3$). Gel permeation chromatography was used to establish the polydispersity of each copolymer, and blends of SID and ISD triblock copolymers were prepared by solvent-casting from tetrahydrofuran and drying at 70°C.

SAXS experiments were conducted on the ORNL 10-m camera and also on the University of Minnesota beamline, both with CuK_{α} X rays. Samples were placed inside an evacuated chamber in the temperature range 45–210°C. Two-dimensional (2-D) diffraction images were corrected for detector response characteristics and background scattering prior to analysis. Azimuthal integration of the 2-D data produced plots of intensity I vs wave vector, $q = 4\pi\lambda^{-1}\sin(\theta/2)$, where λ and θ are the wavelength (1.54 Å) and scattering angle, respectively. SANS experiments were performed on the KWS1 SANS facility at the FRJ2 research reactor in Jülich, with a wavelength of $\lambda = 7$ Å ($\Delta\lambda/\lambda = 0.20$) and also at the National Institute for Standards and Technology (NIST) in Gaithersburg, using $\lambda = 6$ Å ($\Delta\lambda/\lambda = 0.10$).

The smaller wavelength range of the latter facility minimizes instrumental "smearing" effects, to which the "peaks" observed in this study are particularly sensitive. Most intersample comparisons were therefore made on the NIST instrument, though for a given sample run on both facilities (e.g., ISD1), the same ODT was observed within an error of ±1.5°C, and this served as a useful cross-calibration. All data sets were corrected for instrumental sensitivity as described previously and normalized to an absolute (±4%) differential cross section per unit sample volume [$d\Sigma/d\Omega(Q)$ in units of cm^{-1}] by the same pre-calibrated secondary standards.

DMS was used to determine approximate temperatures at which the various block copolymer systems undergo ODTs; these measurements were conducted while increasing the temperature to measure the dynamic elastic modulus.

A series of symmetrical SID and ISD triblock copolymers, with the same volume fraction (~0.33) for each component, were synthesized with number-averaged molecular weights (M_ns) of 9.4×10^{-3} M_n (ISD1), 31.0×10^{-3} M_n (ISD2), 8.5×10^{-3} M_n (SID7), and 7.5×10^{-3} M_n (SID8). The polydispersity, as measured by the ratio of the weight-averaged molecular weight (M_w) to M_n, was typically 1.14, and experiments were performed on the neat triblocks and also on SID/ISD blends. We associated the loss of elasticity via DMS with the ODT temperature (T_{ODT}), which was determined to be 117°C (ISD1), >240°C (ISD2), 227°C (SID8), and 127°C (SID8). A striking feature associated with these results is the 110°C difference in T_{ODT} between ISD1 and SID7, samples with identical compositions and MWs.

The SAXS patterns for each triblock copolymer contain two or more sharp peaks indicative of an ordered structure. Those from samples ISD2, SID7, and SID8 are characterized by the sequence q^*, $2q^*$, $3q^*$, … where q^* is the wave-vector for the lowest order reflection. This pattern reflects a lamellar morphology, though closer examination of the SAXS traces reveals a distinct difference between ISD2 and those from SID7 and SID8. In the former, q^* occurs at nearly half the q value found in the other two, and this effects reflects differences in the lamellar stacking sequences, which could be established from the SAXS data.

For the ISD1 sample, the two diffraction peaks appear with the ratio q^*, $\sqrt{3}q^*$. We identified this morphology as hexagonally ordered cylinders. In addition, a broad

scattering maximum suggests partial mixing between two of the blocks. Based on estimated values for χ between the different monomers, we anticipate preferential mixing of the S and I blocks and minimal D interfacial area.

Based on relative SAXS diffraction intensities calculated for various model structures, we believe that ISD1 contains a quasi-two-domain cylindrical morphology with a partially segregated S+I matrix. Samples SID8 and ISD1 were also examined in the disordered states, and in all cases the ODT is signaled by a discontinuous drop in peak intensity with heating, at the same temperatures identified by DMS. We also explored the consequences of blending sequentially distinct triblocks using samples SID7 and ISD1. These homologous polymers contain equal fractions of each block and nearly identical MWs. DMS experiments on these blends also contain a precipitous drop at a temperature that we associate with the ODT.

Other transitions in elastic response were recorded as the composition increases from 40% to 50% (wt % SID7 in ISD1), where the dynamic elastic modulus (G') jumps two orders of magnitude, and as the composition increases from 85 to 95%, G' reduces by three orders of magnitude. The 85% sample undergoes a transition between 110 and 140°C, while the 95% blend exhibits a small but distinct increase in G′ at 208°C before plummeting at 220°C. We associate these changes with order-order transitions (OOTs).

Insight into the underlying morphologies of these blends was gleaned from SAXS. Between 40 and 85% SID7, a new scattering pattern appears, with two reflections with a relative spacing of $\sqrt{6}q^*$ to $\sqrt{8}q^*$, and corresponding peak intensities of 10:1. These features are characteristics of the "two-domain" gyroid phase. Decreasing the temperature to 70°C increased the magnitude of the $2q^*$ peak at the expense of the $\sqrt{8}q^*$ reflection intensity. We interpreted this as exchange of gyroid for lamellar morphology. On the other hand, heating to 130°C, and subsequently to the T_{ODT}, eliminated the lamellar component, leaving only a gyroid SAXS signal, which persisted until disordering. These findings show that differences in sequencing cause changes in the ordered-state stability, the pathway to disorder, and the nature of the disordered state. In blends of SID7 and ISD1, two triblocks with similar volume fractions and MW, we identified a two-domain gyroid morphology with DMS channels surrounded by a matrix of mixed styrene and isoprene blocks.

Each of the four ABC triblocks examined was synthesized to compare the ordered and disordered states. ISD1 and SID7 were made to compare the ODT temperatures for compositionally symmetric ABC and BAC copolymers. SID8 was made to examine the SID disordered state at an experimentally accessible temperature and ISD2 was prepared to examine the phase behavior of an ISD copolymer where I and S blocks are segregated.

The differences in T_{ODT} can be interpreted by comparing copolymer MWs, block connectivities, and the relative magnitudes of the FH-interaction parameters. These are $\chi_{SI} = 33.0/T - 0.023$; $\chi_{ID} = 43.6/T - 0.010$; and $\chi_{SD} = 68.0/T - 0.037$. Thus, χ_{SD} is the largest χ-parameter, which is forced by connectivity (e.g., for ISD), or muted through separation by the middle block (e.g., for SID). Segregation strength Ψ is usually quantified using a product of χ and the degree of polymerization N. Thus, we may calculate

$$\Psi = \sum_{i \neq j} \chi_{ij} N_{ij}$$

over blocks i and j as 15.1, 12.7, 19.1 and 44.1 for SID8, SID7, ISD1 and ISD2, respectively. This summation illustrates the general deductions that can be made about segregation strength. Although they differ in MW by ~1000 g/mol, the difference in T_{ODT} between SID7 and SID8 is ~95°C. Thus the dependence of T_{ODT} on MW is stronger for ABC triblocks than for diblocks, though the difference in T_{ODT} here is also caused by asymmetry in the composition of SID8. The relatively larger D block of the SID8 copolymer results in fewer heterogeneous segment interactions in the disordered state, thus lowering T_{ODT}.

SID7 disorders at a lower value of Ψ than SID8, and the difference in ODT between ISD1 and SID7 is ~110°C, although the two have similar MW and segment volume fractions. The relative magnitudes of the χ parameters are consistent with this result; because of the energetically unfavorable S-D interactions forced by block connectivity, compositionally symmetric ISD1 disorders at a lower temperature than does SID7. In the disordered state, I-D interactions replace some S-D interactions in the ISD architecture, which stabilizes the melt.

Conversely, upon disordering of SID, S-I and I-D interactions are replaced with the more unfavorable S-D interactions, destabilizing the disordered state. Only after the melt has been sufficiently heated to make the entropic cost for chain confinement greater than the penalty for creating S-D interactions does an SID molecule go through an ODT. The architecture of ISD actually promotes disordering; there is both an enthalpic and entropic benefit to disordering at lower temperatures than SID. This is why Ψ for SID7 is significantly lower than Ψ for ISD1 at the respective T_{ODT}'s.

ISD2 did not show an ODT up to 240°C. The value of Ψ at that temperature is significantly higher than its value at T_{ODT} for any of the other polymers. The large difference between the value of Ψ for ISD2 and those for the other three polymers demonstrates its usefulness as a simple way of quantifying the degree of segregation in a compositionally symmetric ABC block copolymer.

For Ψ in the range 10–20, these samples can be considered close to an ODT, while for Ψ near 50, substantial heating or reduction in MW is necessary for disordering. The relative χ magnitudes suggest that the D blocks would remain segregated while the S + I blocks mix. Peak intensity calculations show how the data lie between the two extremes of a core-shell and a cylindrical morphology. The similarity in scattering from neat ISD1 and low-SID7 composition blends suggests that the blends also form cylinders of D in a matrix of mixed S + I. Gyroid formation over a wide range of compositions and temperatures is a welcome result, since such continuous morphologies are likely to find useful applications.

We also studied an SID triblock (10^{-3} $M_n \sim 42$ with volume fractions of 0.2/0.59/0.21 and $M_w/M_n = 1.1$), blended with mono-disperse PDMS (10^{-3} $M_n = 2.2$) and PS homopolymers (10^{-3} $M_n = 2.4$). The SAXS patterns change as the homopolymers are added and the peak positions shift to lower q, while maintaining their relative positions. When $\varphi = 0.45$, the peaks broaden, and at $\varphi = 0.5$, they regain sharpness but their relative positions change. As more homopolymer is added, the peaks shift to lower q again until $\varphi = 0.65$, where they have nearly disappeared.

Our working hypothesis to explain these changes is that addition of PS and PDMS homopolymers creates a core-shell gyroid structure (up to 30%). As more homopolymer is added, the morphology changes to hexagonally packed core-shell tubes before phase separation at approximately 65 vol %. We attribute the appearance of core-shell structures, and phase separation, to the asymmetry in the χ-parameters, which affects not only the interfacial area between the blocks but also the distribution of homopolymer within the end blocks, making the core-shell morphologies, gyroid, and cylinder more prevalent than the alternating structures observed in other systems. In the limit, this delicate imbalance leads to macroscopic phase separation.

Summary and Conclusions

Differences between compositionally symmetric SID and ISD triblock copolymers have been found in the relative ordered-state stability, pathway to disorder, ordered-state symmetry, and disordered-state scattering. Because of the drive to eliminate unfavorable S-D interactions, ISD disorders at a lower temperature than does SID at comparable compositions and MWs. With heating, lamellar ISD undergoes a mixing of S and I blocks to dilute S-D interactions. This mixing promotes a transition from a three-domain lamellar to a two-domain cylindrical morphology. Heating SID results in a transition to disorder directly from the lamellar state.

Blends of ISD and SID copolymers having approximately equal segment volume fractions and MWs show full miscibility and a synergistic gyroid formation over an extensive composition range. As the weight percent of SID increases, the ordered-state morphology evolves from cylindrical, to gyroid, to lamellar. Relative strengths of interaction parameters help us to deduce that blend self-assembly occurs through mixing of S and I blocks and microphase separation of D blocks.

To date, six presentations of work, supported in part by this project, have been made at national conferences (e.g., American Physical Society, American Chemical Society). A presentation entitled "Structure of Polymer Melts," containing data from this project, was given to the Division of Material Sciences & Engineering Condensed Matter Physics and Materials Chemistry Review on September 12, 2000.

A new project, aimed at quantifying χ_{AB}, χ_{AC}, and χ_{BC} in the commercially important saturated hydrocarbon triblocks, has been spawned from our research and will form the basis for designing block copolymers with prescribed amounts of glassy, rubbery, and semicrystalline elements with specified linear and non-linear mechanical properties.

A proposal entitled "Integrated Design of Nanostructured Multi-Block Copolymer Materials" was submitted in January 2001 to the DOE Office of Science under the Nanoscale Science, Engineering, and Technology (NSET) Initiative. It reached the final round of reviews but was not funded. Another submission via a recent DOE NSET call (11-13-2001) is under consideration. A Multidisciplinary University Research Initiative (MURI) proposal in collaboration with the University of Minnesota has been submitted to the U.S. Army.

Publications Derived from This Project

M. Sugiyama, T. A. Shefelbine, M. E. Vigild, and F. S. Bates, "Phase Behavior of an ABC Triblock Copolymer Blended with A and C Homopolymers," *J. Phys. Chem. B*, in press.

C. M. Hardy, F. S. Bates, M.-H. Kim, and G. D. Wignall, "Model ABC Triblock Copolymers and Blends Near the Order-Disorder Transition," *Macromolecules*, in press.

E. W. Cochran and F. S. Bates, "Design of Model Saturated Hydrocarbon ABC Triblock Copolymers Near the Order-Disorder Transition," in preparation for submission to *Macromolecules*.

Investigation of Oxidation Resistance in Titanium Aluminides Through Z-Contrast Scanning-Transmission Electron Microscopy

S. J. Pennycook,[1] M. F. Chisholm,[1] and S. K. Varma[2]
[1]*Solid State Division*
[2]*The University of Texas at El Paso*

The purpose of this project was to determine the mechanisms by which niobium provides oxidation resistance in titanium aluminides. The oxidation resistance and ductility of titanium aluminides can be significantly improved by the addition of alloying elements. Niobium and chromium are the two common alloying elements tested for this purpose. However, niobium has been shown to be much more effective although the reason for this has not been established. Microcharacterization was carried out using the facilities for Z-contrast scanning transmission electron microscopy at ORNL during a summer visit by Professor Varma.

Introduction

Titanium aluminides are of great interest for substituting conventional nickel-based superalloys in the aircraft industry because of the potential weight savings. While numerous alloys have been investigated in the past, alloys from the Ti-Al-niobium system are particularly attractive due to their resistance to oxidation. Prior work by Professor Varma focused on alloys containing 4, 8, 11, and 12 at % niobium. Oxidation curves indicate that the addition of more than 8 at % niobium does not provide any extra resistance against oxidation in air at temperatures of 800–100°C. The key to understanding the mechanisms of oxidation resistance lies in the identification of oxide phases in the scale and the adherence of the scale to the base metal. Transmission electron microscopy (TEM) revealed a very complex microstructure. In fact, there is an evidence of the formation of a new phase in an aluminum-depleted zone located between the scale and the base metal. However, these studies were not able to unambiguously determine the role of the niobium due to a lack of detailed information on the distribution of niobium. Since the atomic number Z of niobium is 41, much higher than the component titanium (Z = 22) or aluminum (Z = 13), it was felt that this would be an excellent new application of the technique of Z-contrast microscopy to an important technological problem.

Technical Approach

The proposed approach was to use the technique of Z-contrast scanning transmission electron microscopy (STEM) to locate the niobium in a series of alloys and thus determine its role in oxidation resistance. Z-contrast STEM is a technique that has high sensitivity to elements of high atomic number. It provides in effect an elemental map with a much higher signal level than conventional microanalysis. In the STEM, the image resolution is controlled by the size of the scanning beam; in our case we have a world record of 0.13 nm, which is sufficiently small to resolve the atomic structure of these alloys. The Z-contrast image is formed by using an annular detector to collect scattered electrons. The signal from this detector is used to modulate the intensity on a TV screen as the probe scans, forming in effect a map of the number of scattered electrons. The scattering cross section is proportional to Z^2, so high sensitivity to niobium is expected. Also, because of our very high spatial resolution, in contrast to previous studies, we would be sensitive to single monolayers of niobium at grain boundaries or interfaces.

A series of samples were made with niobium concentration of 4–14 at % at the University of Texas, El Paso, and studied by conventional TEM. Heat treatment experiments in such alloys included a process of homogenization at 1200°C for hours, quenching in water followed by aging in a range of temperatures from 800 to 1000°C for 4 h, and again quenching in water. The TEM studies revealed phase transformations taking place at the prior grains containing a lamellar mixture of γ (Ti-rich) and α_2 (Al-rich) phases. The grains nucleated at these boundaries have been identified as those containing γ in massive form and grains containing much coarser lamellar structure. Although the microstructure was strongly dependent on niobium content as the metal forms an alloy with the lamellar phases, its distribution and effect on properties could not be determined from these studies alone. These specimens were therefore brought to ORNL.

Results and Accomplishments

A significant fraction of the time spent at ORNL was used in selecting the most appropriate samples for the Z-contrast study. Clearly to achieve atomic resolution, it is necessary to have the grain oriented along a major crystallographic direction. For grain boundary segregation studies, two neighboring grains must be oriented appropriately in order to have atomic resolution at the interface and the best sensitivity for detecting niobium. Samples were surveyed using a number of facilities at ORNL. (1) A scanning electron microscope in the Solid State Division equipped with a thin window energy-dispersive X-ray detector was used with the assistance of N. Dudney to obtain compositions of oxide scales. (2) A Philips EM400 conventional transmission electron microscope in the Solid State Division was used to survey TEM specimens for suitable orientations and thicknesses. Figure 1 shows an image of a Ti–44% Al alloy obtained with this microscope showing a region undergoing transformation from the γ phase to $\gamma + \alpha_2$ phases. (3) A Philips CM200 analytical transmission electron microscope in the SHARE facility of the Metals and Ceramics Division was used to profile niobium content in grains. Niobium concentrations were relatively uniform within the lamellae, but this microscope did not provide sufficient spatial resolution to give a detailed analysis at the interface. (4) The VG Microscope HB603U in the Solid State Division was used to provide atomic-resolution Z-contrast images of the ordered structures. Because of the large grain size of these alloys and the large number of possible orientations in a polycrystalline sample, there are only a few grains in each TEM specimen, and we were unable to find any regions of the samples in which a suitably oriented interface was located. Nevertheless, we were able to resolve the ordered structure as shown in Fig. 2.

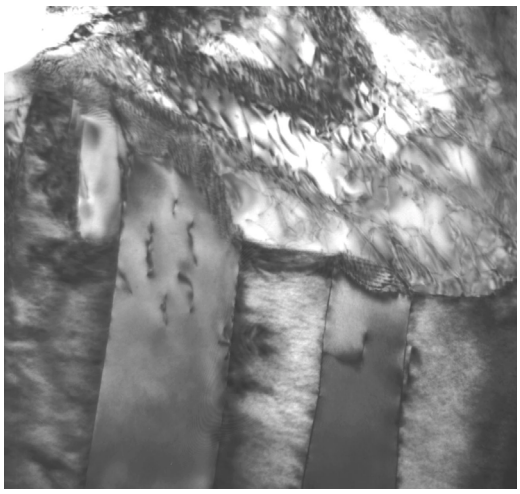

Fig.1. TEM image of a Ti–44% Al alloy showing transformation from the γ phase (top) to $\gamma + \alpha_2$ phases (the lamellar structure, bottom).

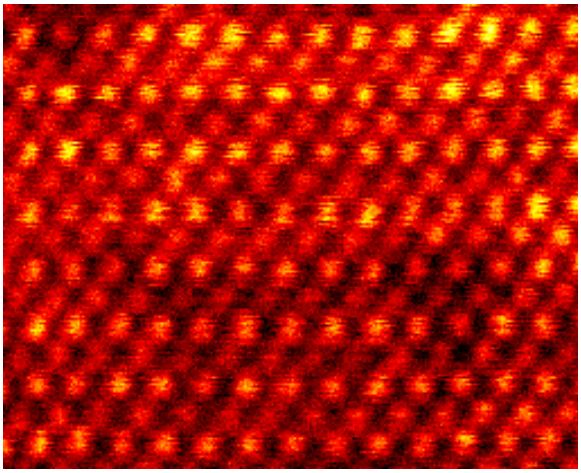

Fig. 2. Atomic resolution Z-contrast image of a Ti–44% Al–8% niobium alloy showing the ordered structure. Every other horizontal plane is bright, indicating enrichment by titanium or niobium.

Summary and Conclusions

Although we were not able in the time available to obtain a clear result concerning the mechanism of the oxidation resistance, the work did show the potential of Z-contrast imaging for directly revealing the structure of these ordered alloys. The ability to distinguish the high-Z atomic columns from low-Z columns shown in Fig. 2 is a unique advantage of the Z-contrast method. Further studies are needed to correlate the ordering with the fraction of niobium present. Also, we are now installing an energy loss spectrometer on this microscope which would allow atomic-resolution composition analysis to show directly if the bright planes are the sites of niobium or are just titanium rich.

It is thought very likely that the role of dopants or alloying additions such as niobium is to modify the atomic structure within just a few monolayers of the interface. Simply changing the structure from ordered to disordered has a strong effect on properties such as diffusion (necessary for oxidation) and the slip of dislocations (necessary for ductility) and therefore is very likely to be at the heart of the mechanisms of oxidation resistance and mechanical properties. Prior studies by conventional microscopy have not been able to see the ordered structure at this level of resolution, which we believe is the reason that the role of niobium in mechanical properties or oxidation resistance is not understood. We did not anticipate being able to fully solve this complex problem in one 2-month visit, but sufficient progress was made to demonstrate the potential for Z-contrast microscopy on these materials, and we are now in a competitive position to submit proposals on this subject.

Materials Science of Novel Carbon and Graphite Materials

J. W. Klett, A. D. McMillan, N. C. Gallego, and T. D. Burchell
Metals and Ceramics Division

It is proposed that a preliminary study of key structure/property relationships be undertaken in an effort to elucidate some of the fundamental physical processes occurring in a series of novel nanostructured carbon and graphite materials. The results of this work will provide needed data and the basis for future proposals to the DOE and the Department of Defense.

Introduction

Carbon and graphite materials encompass a broad range of structures—from highly ordered crystalline materials to disordered amorphous materials. One class of carbon materials, graphite foam, takes advantage of the high degree of crystalline order that may be developed in mesophase pitch-derived graphite. This material exhibits unique and interesting properties because of structural or molecular phenomena occurring at the nanoscale.

In previous research, Bovenkerk et al.[1] demonstrated that by producing chemical-vapor-deposition (CVD) diamond structures with isotopically pure carbon atoms (either ^{12}C or ^{13}C), thermal conductivities can be increased by up to 50%. Since heat is conducted in carbon (either graphite or diamond) by phonons, anything that decreases the phonon mean free path (i.e., lattice vibration modes) will decrease the thermal conductivity. In 98% of natural diamonds (type Ia), nitrogen impurities act as phonon scattering centers and, therefore, reduce the thermal conductivity to about 800 W/m·K, compared to nearly 2500 W/m·K for perfect diamonds (Type II). In polycrystalline diamonds (or man-made CVD diamond films), defects such as twins, grain boundaries, vacancies, and dislocations reduce the phonon mean free path, yielding a thermal conductivity of approximately 800 W/m·K. Furthermore, the atomic weight of the atoms also acts as a defect. A different atomic weight will result in different bonding strengths, which then result in different vibrational modes of the atoms, thereby affecting the mean free path of the phonons. To demonstrate this, Bovenkerk et al.[1] produced CVD diamond films that were isotopically pure (i.e., pure ^{12}C diamond films). The resulting thermal conductivity was measured to be about 1200 W/m·K, compared to 800 W/m·K for the diamond with the normal distribution of isotopes. Developing this further would go far in advancing the thermal properties of many carbon products.

The graphite foam developed at ORNL exhibits a high thermal conductivity at low density.[2–6] This results in a carbon material with an extremely high specific thermal conductivity that is attractive for thermal management applications in weight-sensitive environments. Moreover, the open cell structure of the foam imparts a large surface area to the foam. This, combined with the foam's high thermal conductivity, makes the material an ideal candidate for the core of heat transfer devices such as radiators, heat sinks, evaporative cooling, and phase change devices. Furthermore, the ability of the graphite foam to intercalate lithium, and absorb acoustic energy, makes the foam a candidate for many nonthermal management applications.

In certain applications, the ability to advance the materials development is hindered by a lack of fundamental insight into the key structure/property relationships in these carbon materials. For example, the thermal conductivity of graphite foam is controlled by phonon scattering from crystal defects in the graphite lattice such as collapsed vacancy loops. The extent of structural imperfection is known to be a function of graphitization temperature in well-ordered graphitic materials. Understanding the relationship between graphitization temperature, the degree of crystal perfection, and the thermal conductivity is thus critical to the further development of this material. This carbon-based material exhibits microstructural order (or disorder) at the nanometer scale, and thus the proposed research corresponds to ORNL's nanoscale science research thrust area.

Technical Approach

Graphitization Heating Rate Effects on the Physical Properties of Graphite Foam

For many carbon materials, the heat treatment rate during graphitization is critical to optimizing the material properties. Heating at a rate of approximately 0.1°C/min to

2800°C (the graphitization temperature) is not uncommon. However, the carbon foam is currently heated at a rate of approximately 10°C/min during the graphitization cycle. It is proposed to evaluate/study the influence of heating rate during graphitization on key properties of the foam such as density, thermal diffusivity, and crystalline parameters.

Several billets of foam were produced utilizing two heating rates during foaming (3.5°C/min and 10°C/min). These samples were then carbonized at a heating rate of 0.2°C/min. The samples were cut into 5/8-in. cubes in a regular pattern throughout the sample, and the density was measured on each cube. Then, these foams were heated to the graphitization temperature utilizing five heating rates (0.5, 1, 5, 10, 15°C/min). Key material properties, such as degree of graphitization, crystallographic structure, thermal diffusivity and density, were measured on several samples of foams graphitized at each heating rate. These data will be used to determine the optimal heating rate during the graphitization of the foams and, therefore, optimize the thermal properties of the foams.

Development of Isotopically Pure Carbon CVD

It is proposed to demonstrate this technique for enhancing the thermal properties of CVD graphite layers in carbon composites and carbon foams. Carbon CVD is typically used to densify carbon composites and carbon foams. By producing a CVD layer of matrix, which is up to 50% more thermally conductive, enhancements to materials ranging from aircraft brakes to thermal management substrates and CVD-rigidized graphite foams can be realized. It is also theorized that the resulting isotopically pure carbon matrices will also exhibit enhanced mechanical properties as the resulting material will exhibit very uniform bond strengths, thereby reducing stress concentrators within the structure. If it is demonstrated that graphite can be similarly enhanced through isotopic purification (i.e., producing graphite from an isotopically pure starting material), then it will be possible to produce an isotopically pure feedstock for the production of graphite foams. This could result in bulk thermal conductivities approaching 270 W/m·K at an apparent density of 0.5 g/cc. Such an enhancement in material properties of the foams would benefit the energy efficiency of many devices. The research will involve depositing standard CVD graphite layers on a carbon substrate and also depositing isotopically pure CVD layers on a similar substrate. The materials will be characterized with a scanning tunneling thermal microprobe to determine the effective thermal conductivity of the CVD graphite films. The films will also be characterized with X-ray diffraction (XRD) to determine the effects of isotopic purity on the crystallographic structure of the film.

Results and Accomplishments

Graphitization Heating Rate Effects on the Physical Properties of Graphite Foam

The first characterization of the foams was the measurement of the density uniformity of the foams after carbonization (1000°C). As elaborated earlier, the foams were made with two different foaming rates (3.5°C/min and 10°C/min). Also, the billets were taken from different positions in the furnace (as illustrated in Fig. 1), specifically the top position and the bottom position. This would give an understanding of the temperature uniformity within the furnace and its effects on the resulting foam. As all samples within a billet (pan) experienced the same processing rates and temperatures up through carbonization, this was a good measure of the density uniformity. It was observed that there was a significant effect on density uniformity (smaller deviations) by the position in the furnace. While there appeared to be a slight effect on density uniformity due to the foaming rate, this effect was small compared to the effect of the position of the pan in the furnace. This implies that the temperature at the bottom of the furnace (most likely lower temperature) during the foaming is not sufficient to produce uniform temperature profiles in the foam, thereby leading to nonuniform foam density plots.

The density of the individual cubes of each billet was measured. It was evident that the samples located at the top of the furnace have a more uniform density. However, it was also noted that the samples made with the lower foaming rate of 3.5°C/min exhibited higher overall densities. Perhaps the lower foaming rate allows bubbles to collapse during the foaming, thereby yielding thicker ligaments and denser foams. This is illustrated in Fig. 1 (a comparison of SEM images of foams located in the same part of the furnace but with different foaming rates).

Four cubes from each billet were separated and fired to 2800°C at five different heating rates (0.5, 1, 5, 10, and 15°C/min). The thermal properties of the samples were then measured in all three directions (z, y, x) with Xenon flash diffusivity, and the thermal conductivity of the samples was calculated. These data indicate that the thermal conductivity is directly related to the graphitization heating rate. However, it is not understood why there is a maximum at 1°C/min. The samples graphitized (or heat treated) at 0.5°C/min experienced a furnace outage when the samples were only at 750°C (less than the previously experienced carbonization temperature), and the furnace cooled to room temperature in several hours overnight. This outage obviously imparted a cooling rate greater than the 0.5°C/min heating rate and perhaps is the reason for the apparent lower thermal conductivities in all directions for this heating rate. It was anticipated that the lowest heating rate would provide the best thermal conductivity.

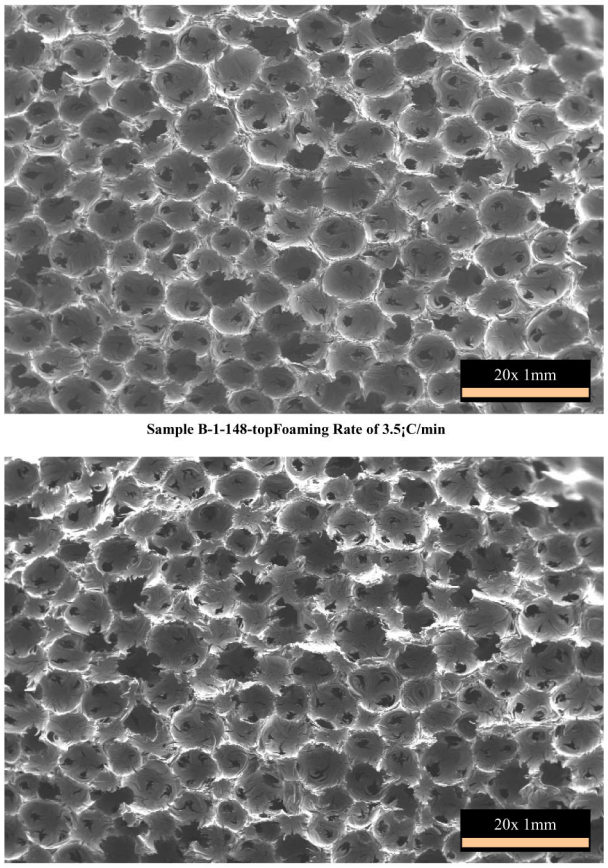

Fig. 1. Comparison of foams made at different foaming rates.

The effect of the location of the foam in the foaming furnace on the final thermal properties is also noteworthy. It is clear that in the Z-direction (the direction with the highest conductivity), both billets that were located in the top of the furnace exhibited the highest overall thermal conductivity, irrespective of foaming rate. However, it is also evident that the foaming rate does affect the final thermal properties, with the lower foaming rate yielding graphitized foam with the higher thermal conductivity. While these trends are generally true for the x and y directions, the effects are smaller due to the lower thermal conductivites.

The crystalline parameters [interlayer spacing (d_{002}), crystal stacking height ($Lc_{,002}$) and the crystal coherence length ($La_{,100}$)] were measured with XRD. In graphitic materials (d-spacings between 3.354 and 3.440 nm), it is generally true that the overall thermal conductivity of the graphite material will increase as the d-spacing approaches that of perfect graphite (3.354 nm). However, as the d-spacing approaches 3.354–3.360, the effect of phonon-phonon scattering is more prevalent and the thermal properties are related to the coherence length. This is the mean free length between lattice edges that scatter phonons and decreases the thermal conductivity. This effect can be observed in the foam samples prepared in this study. All the samples (all heating rates) exhibited d-spacings between 3.358 and 3.368 nm as anticipated. Furthermore, there does not appear to be a strong correlation between either the foaming rate, the position in furnace, or the graphitization rate on the interlayer spacing. This trend also holds true for the stacking height. However, as anticipated, the coherence length shows the same trend as the thermal conductivity in the z direction. It was seen that the samples made in the top of the furnace exhibit higher thermal conductivities than those in the bottom of the furnace. Also, it is evident that the samples made with a lower foaming rate exhibit higher thermal conductivities. Last, it is also clear that as the graphitization rate increases, the coherence length decreases with the same trend that the thermal conductivity decreases

Last, the samples were examined prior to and after graphitization with a scanning electron microscope (SEM) in the same spot on each sample. This was performed to determine if the graphitization rate was affecting the physical structure of the pores, rather than just affecting the crystal structure. Unexpectedly, the most significant effect was viewed in the lower magnifications. It appeared that the samples with the lower graphitization rate exhibited less overall structural change and morphing of the bubbles than that seen at the higher heat treatment rates. When viewed in the higher magnifications (examining individual ligaments), the samples with the faster heat treatment rates did appear to exhibit larger and more frequent microcracks in the walls and ligaments of the foams. However, these effects are inconclusive as there is microcracking in all the samples after graphitization. In light of the data from the coherence length of the crystals, it appears that the effect on the crystal structure has more of an affect on the thermal properties than the structure changes on the foams. Perhaps, the structural changes in the foams affect the mechanical properties in the same significant manner as the crystal properties of the ligaments affect the thermal properties. In other words, thermal conductivity is dominated by the crystal properties and the mechanical properties are dominated by the physical structure of the foams. It is fortunate that it appears, through the SEM visualization, that the trend will be similar for both phenomena (i.e., slower heating rates will increase thermal conductivity and mechanical properties).

Development of Isotopically Pure Carbon CVD

A lecture bottle (10 L) of ^{12}C, 99.999% methane gas was procured from Cambridge Isotope Laboratories. The bottle was placed in-line on the CVD furnace used in previous work. Leak checks were performed. Each foam sample was weighted before being placed in the CVD furnace. The furnace was then programmed at a given

heating rate, and the gas was controlled at a given flow rate to allow deposition for nearly 1 h. Approximately 10 min into the run, a check was made on the progress; the lecture bottle was already empty. Samples were removed and weighed; less than 0.5% mass by weight was deposited, resulting in a CVD layer that was so thin that it was difficult to detect. Unfortunately, this gas is costly and we were unable to procure additional material to run the experiment again. However, if we could buy several hundred liters of gas, which would allow several experiments with significant deposition, a redesign of the furnace may be necessary. Typically, the furnace furniture also receives a deposition layer; however, due to the high cost of the isotopically pure methane, the furnace interior would be redesigned to allow more efficient deposition of carbon directly onto the samples, rather than the furnace furniture.

Summary and Conclusions

There were several conclusive results from the studies of the graphitization rate on the foams. First, the temperature uniformity and homogeneity of the foaming furnace is critical as it was found that the samples made at the top of the furnace exhibited the highest thermal conductivities. Second, it was evident that the foaming rate of the precursor pitch is critical as it was found that samples foamed at the lower rate exhibited higher thermal properties. Last, it was found that the graphitization rate was critical to the thermal properties and that higher heating rates tend to disrupt the crystal structure (specifically the coherence length) and decrease the thermal properties. It was also found that the position in the furnace and the foaming rate exhibited a larger effect on the thermal properties than the graphitization rate; however, the graphitization rate did have a significant effect on the final properties of the foams.

References

[1]Bovenkerk et al., U.S. Patent 5,540,904.

[2]J. W. Klett, A. D. McMillan, and R. Ott, "Heat Exchangers for Heavy Vehicles Utilizing High Thermal Conductivity Graphite Foams," Proceedings of the Society of Automotive Engineering Government/Industry Meeting, June 19–21, 2000, Renaissance Hotel, Washington, D.C., USA.

[3]J. W. Klett, L. Klett, T. D. Burchell, and C. Walls, "Graphitic Foam Thermal Management Materials for Electronic Packaging," Proceedings of the Society of Automotive Engineering Future Car Congress, Crystal City, Washington, DC, April 2–6, 2000.

[4]J. W. Klett and B. Conway, "Thermal Management Solutions Utilizing High Thermal Conductivity Graphite Foams," Proceedings of the 45th International SAMPE Symposium and Exhibition, Long Beach, CA, May 21–25, 2000.

[5]J. W. Klett, R. Hardy, E. Romine, C. Walls , and T. D. Burchell, "High-Thermal-Conductivity, Mesophase-Pitch-Derived Carbon Foams: Effect of Precursor on Structure and Properties," ***C****arbon* **38**, 953 (2000).

[6]J. W. Klett, "High Thermal Conductivity Mesophase Pitch-Derived Graphitic Foams," *Composites in Manufacturing* **14**, no. 4 (1999).

Computation with Arrays of Quantum Dots

J. Barhen,[1] Y. Braiman,[1] D. J. Dean,[2] L. Maya,[3] V. A. Protopopescu,[1] N. S. V. Rao,[1] M. R. Strayer,[2]
T. G. Thundat,[4] and J.C. Wells[1]
[1]*Computer Science and Mathematics Division*
[2]*Physics Division*
[3]*Chemical Sciences Division*
[4]*Life Sciences Division*

The goal of this proposal is to develop a quantum-dot (QD) array for carrying out innovative computations to address the information processing needs of future intelligent systems. The effort includes the actual fabrication of 2-nm gold clusters, device architecture, device simulation, development of a computational model, and novel applications. Innovative and unconventional paradigms underlie the different stages of the project. Regular array geometry will be achieved by the development of techniques for the programmed assembly of appropriately functionalized gold clusters to preselected locations along stretched strands of engineered DNA sequences. Our applications include the implementation of neuromorphic algorithms for pattern recognition.

Revolutionary advances in nanoscale computing, communication, detection, and sensing subsume a profound understanding of the dynamics and properties of small arrays of quantum structures, including quantum dots, tunneling junctions, etc. Such arrays produce multistable robust behavior that can be exploited for unconventional computational concepts. The implementation of neuromorphic algorithms appears to offer a great promise. Long-term targeted benefits would include unprecedented computational performance in applications such as associative retrieval, image processing, and optimization, along with reduced size and power consumption. New, unconventional algorithms are being developed that exploit the collective properties of a QD array and are capable of fully using the technology of such emerging nano-devices.

Over the past months, we have made considerable progress toward this goal to date. In particular, we have

(1) synthesized ensembles of gold nanoclusters with a variety of chemical functionalities;
(2) developed novel self-assembly techniques to produce large-scale two-dimensional assemblies of these nanoclusters and measured current-voltage characteristics through these arrays in which both Coulomb blockade and negative-differential resistance phenomena are observed; and
(3) achieved leading-edge results in the attachment of these nanoclusters at pre-defined locations upon engineered strands of DNA.

We understand that ours is the first group to covalently attach nanoparticles in such a regular manner at internal sites along long strands of DNA.

The interest we have received from external colleagues and program managers has confirmed our view that programmed assembly of structured nanomaterials via DNA templates is of profound importance for future development of nanoscale engineering and technology. We have also simulated the structure and charging of metal clusters to compute from first-principles device characteristics and computed the current-voltage characteristics in arrays of such nanoconductors by considering the phenomena of single-electron tunneling.

Since we began our project 2 years ago, opportunities for R&D in computational nanotechnology and nanophase materials science have become more exciting. Our concepts in the programmed assembly of nanoparticles along DNA templates will soon be applied in spin-off activities in revolutionary computation and nonstructural photonics, funded by DOE-SC Office of Basic Energy Science and DOE Defense Program, while our concepts in neuromorphic computing with arrays of metal nanoclusters will be applied to enable self-evolving networks of single-electron switching latches, funded by the Office of Naval Research and the National Science Foundation.

Publications Derived from This Project

L Maya et al., "Polymer Mediated Assembly of Gold Nanoclusters," *Langmuir* **16**, 9151 (2000).

G. Muralidharan et al., "Structure and Electrical Properties of an Assembly of Au Nanoclusters," *Materials Research Society Symposium Proceedings*, Vol. 635, Fall 2000.

K. Stevenson et al., "Site-specific Attachment of Gold Nanoparticles to DNA Templates," *Materials Research Society Symposium Proceedings*, Vol. 635, Fall 2000.

J. C. Wells et al., "Programmed Assembly of Nanostructures for Computing via DNA Templates," pp. 263–268 in *SCI-2000*, Vol. XI, Orlando, Florida, July 2000.

J. Barhen et al., "Neuromorphic Pattern Recognition Using Arrays of Quantum Dots," pp. 257–262 in *SCI-2000*, Vol. XI, Orlando, Florida, July 2000.

L. Maya et al., "Assembly of gold nanoclusters on silicon surfaces," *Langmuir* (submitted 2001).

"Smart" Nanocomposite Layers Formed by Ion Implantation

L. A. Boatner and T. E. Haynes
Solid State Division

The goal of this project is to develop an entirely new family of nanocomposite materials based on the use of ion implantation and thermal processing to create "smart" surfaces consisting of "active" nanometer-scale precipitates in the near-surface region of inactive substrates. The new fundamental physical properties of these materials that have been discovered in the course of this project will be applied to applications that support overall DOE missions and projects.

Smart surface nanocomposites consisting of an embedded layer of nanometer precipitates in a host matrix represent a new materials state with unique properties. These materials are created using ion implantation and thermal processing. In these nanocomposites, each precipitate is a faceted single crystal that is aligned with every other precipitate and physically isolated (no interparticle grain boundaries). Compound nanoparticles can be created. The smart nature arises from "active" precipitates in which large property changes at a phase transition provide "feedback" leading to the smart interaction. New physics and effects in these smart nanocomposites arise from the size of the precipitates and nanophase particle-particle or particle/host interactions. The smart surface nanocomposite concept is original to ORNL, and its feasibility was established by the creation of several new types of magneto-optically active surfaces that incorporate nanoparticles of ferromagnetic, semiconducting, and metal-insulator-transition materials in a variety of hosts. The overall objectives are to exploit our recent advances by extending the approach to provide new functionalities (e.g., via the formation of piezoelectric, magnetostrictive, and other active precipitates), to understand the basic physics of these new materials, and to develop new applications including thin-film and fiber-optic devices.

Smart embedded nanocomposite materials have several important advantages over conventional materials including the following: the physical properties of the nanocomposite can be optimized by controlling the particle size; useful properties of two or more materials can be combined into one integrated structure; and embedded, active nanoparticles are protected from the environment. A partial listing of the technical accomplishments of this project is given as follows:

1. Near-surface ferromagnetic nanocomposites have been formed in which chemically ordered FePt precipitates were created in Al_2O_3, SiO_2, MgO, and YSZ hosts. These systems exhibited coercive fields up to 30 kG for single-domain particles, and they are of interest for use in the development of new magnetic data storage materials. In the case of FePt nanoparticles in Al_2O_3, MgO, and YSZ, the particles are crystallographically oriented.
2. We have discovered that through the ion implantation of nanophase ferromagnetic precipitates such as Co it is possible to dramatically increase the coercive field and to move the particles out of the superparamagnetic regime—without significantly altering the particle size.
3. We have shown that it is possible to exploit our ability to create crystallographically oriented nanophase precipitates to form magnetic layers whose properties are those that are desirable for "perpendicular" magnetic data storage.
4. We have discovered that it is possible to use ion implantation and thermal processing to form multicomponent surface nanocomposites by creating distinct particle assemblages based on the utilization of two or more immiscible precipitate materials.
5. We have shown that, in the case of CoPt and FePt ferromagnetic particles, the coercive field is a strong function of the annealing time, temperature, and implantation dose, leading to a means of controlling and tailoring the coercive field.
6. We have discovered a new process for forming surface nanocomposites through the solid-state chemical exchange of implanted and host lattice ions and the subsequent reaction of the host ions with a second implanted species to create a new type of nanocomposite surface.
7. Nanocomposite surfaces have recently been formed in which giant magnetostrictive precipitates of oriented Fe_3Pt nanoparticles are embedded in Al_2O_3 and SiO_2.

8. A giant hysteresis effect has been discovered in the case of VO_2 nanoparticles embedded in fused SiO_2. This effect has a number of potential applications in the field of optical switches, attenuators, sensors, and as an optical data storage medium.
9. We have discovered methods for controlling and tailoring the phase transition temperatures and hysteresis properties of VO_2 nanoparticles by using ion implantation to dope the precipitates with certain impurities.
10. We have discovered and developed the theory for a new magneto-optical effect in the case of ferromagnetic nanoparticles and have also demonstrated and theoretically modeled the effect of interparticle magnetostatic interactions in the case of Fe nanoparticles embedded in a YSZ host.

Publications Derived from this Project

J. Lian, L. M. Wang, S. X. Wang, J. Chen, L. A. Boatner, and R. C. Ewing, "Nanoscale Manipulation of the Structure of Pyrochlore: New Composite Ionic Conductors," *Physical Review Letters* **87**, 145901 (2001).

A. Meldrum, R. F. Haglund, Jr., L. A. Boatner, and C. W. White, "Nanocomposite Materials Formed by Ion Implantation," *Advanced Materials* **13**, 1 (2001).

C. W. White, S. P. Withrow, J. D. Budai, L. A. Boatner, K. D. Sorge, J. R. Thompson, K. S. Beaty, and A. Meldrum, "Ferromagnetic FePt Nanoparticles Formed in Al_2O_3 by Ion Implantation," *Nuclear Instruments and Methods in Physics Research B* (accepted for publication).

A. Meldrum, L. A. Boatner, and R. C. Ewing, "Size effects in the irradiation-induced crystalline-to-amorphous transformation," *Physical Review Letters* (accepted for publication).

R. Lopez, L. A. Boatner, T. E. Haynes, R. F. Haglund, and L. C. Feldman, "Enhanced hysteresis in the semiconducting-to-metal phase transition of VO_2 precipitates formed in SiO_2 by ion implantation," *Applied Physics Letters* **79**, 3161 (2001).

S. Honda, F. A. Modine, A. Meldrum, J. D. Budai, T. E. Haynes, and L. A. Boatner, "Magneto-optical effects from nanophase a-Fe and Fe_3O_4 precipitates formed in yttrium-stabilized ZrO_2 by ion implantation and annealing," *Applied Physics Letters* **77**, 711 (2000).

S. Honda, F. A. Modine, T. E. Haynes, A. Meldrum, J. D. Budai, K. J. Song, J. R. Thompson, and L. A. Boatner, "The Formation of High-Coercivity, Oriented Nanophase Cobalt Precipitates in Al_2O_3 Single Crystals by Ion Implantation," in Nanophase and Nanocomposite Materials III, ed. by S. Komarneni, J. C. Parker, and H. Hahn, *Mat. Res. Symp. Proc*. **581**, 71–76 (2000).

A. Meldrum, L. A. Boatner, C. W. White, and R. C. Ewing, "Ion Irradiation Effects in Nonmetals: Formation of Nanocrystals and Novel Nanocrystal Microstructures," *Materials Research Innovations* **3**, 190 (2000).

A. Meldrum, L. A. Boatner, and C.W. White, "Nanocomposites formed by ion implantation: Recent developments and future opportunities," *Nuclear Instruments and Methods in Physics Research* **B178**, 7 (2001).

L. A. Géa, J. D. Budai, and L. A. Boatner, "Formation and Phase Transition of VO_2 Precipitates Embedded in Sapphire," *J. Mater. Res.* **14**, 2602 (1999).

S. Honda, F. A. Modine, T. E. Haynes, A. Meldrum, J. D. Budai, and L. A. Boatner, "Magnetic properties of a thin layer of monodomain iron particles," *Physical Review B*, in press.

A. Meldrum, C. W. White, R. A. Zuhr, and L. A. Boatner, "Metal nanocrystals in silicon: Void formation and hollow particles," *Journal of Materials Research* **16**, 2670 (2001).

Self-Organized Formation of Quantum Dots: New Physics, New Chemistry, New Technology

Z. Y. Zhang, J. F. Wendelken, and J. Shen
Solid State Division

This project proposed to seize a unique opportunity to make major advances in nanoscale science, engineering, and technology by solving one persistent bottleneck problem of the field: mass production of quantum dots (QDs) with narrow size and uniform spatial distributions. The project is focused on demonstrating the wide applicability of a conceptually new synthesis method conceived at ORNL. The method, called buffer layer and charge-assisted growth (BLC), takes full advantage of simple physical laws (Coulomb repulsion) and surface growth kinetics to enable the formation of QDs of almost any material on any substrate. The discovery of the BLC method (U.S. Patent 6,313,479) has offered unprecedented opportunities for fundamental and applied research in nanoscale science and technology. Using this method, we have achieved the fabrication of two important classes of QD arrays–magnetic (iron) QDs on either metal (copper) or semiconductor (silicon) substrate and germanium QDs on silicon. In both cases, the QDs are in novel configurations characterized by the absence of a wetting layer; these configurations are most desirable for basic research as well as for potential applications in memory, optical, and nanoelectronic devices.

This project has both theoretical and experimental components. On the theory side, we have simulated the growth patterns of QD arrays with the use of an inert gas buffer layer with and without charging, demonstrating that the charging effect is dramatic.[1] During the first 2 years, experimental work has focused first on the details of the technique for growth of QDs via the BLC approach. This work was performed both at The University of Tennessee and at ORNL on two new experimental growth and analysis systems that were built during the first year.

Initial efforts were highly successful with the achievement of QDs of iron on copper and silicon substrates with a reduced size and narrower size distribution than can be obtained without the charging step. The size and density of the QD distribution could be controlled by changing the buffer layer thickness, deposition rate and amount, and charging procedures. Although, so far none of these parameter variations led to the ideal ordering predicted by theory, some indication of ordering was indeed indicated in lines of QDs in localized regions. A search of the factors inhibiting the spatially ordered formation of the QDs experiments was then performed in one of the new systems which is equipped with a variable temperature atomic force microscope (AFM). This allowed direct imaging of the surface of the solid xenon buffer layer at a temperature of 25 K. Our findings here may indicate the key problem. The surface of the xenon is found to be rougher than expected. We have not solved this problem but will continue efforts when more time is available with the variable temperature AFM.

Although we have not as yet been able to form QDs that are highly ordered spatially, this approach offers the possibility of creating many useful structures for either experimental or applied purposes. One notable success has been in the use of the buffer layer technique to create a controlled nanostructure of magnetic iron QDs in a study of low dimensional magnetism. This is a remarkable success since iron cannot be made into QDs on Cu(111) with any other growth methods. The magnetic characterization of the iron dots reveals surprising magnetic stability at elevated temperatures (up to 140 K), which is now understood to be a result of large magnetic anisotropy and dipolar interaction between the dots. With the addition of buffer layer technique, we have now mastered a set of novel methods that enable us to grow two-dimensional (2-D), one-dimension, and zero-dimensional magnetic nanostructures on a common template such as Cu(111) and W(110). Direct comparison of the magnetic properties of these three structures has shown a surprising nonmonotonic behavior as a function of the system dimensionality.[2]

Another potentially very useful structure has been created recently using the same approach with germanium QDs deposited on silicon. For the first time, germanium QDs have been created without the usual wetting layer and with a size distribution one order of magnitude smaller than can be obtained with conventional growth techniques. This smaller size and lack of a wetting layer will result in improved quantum confinement with possibly enhanced optical properties. Measurements are being performed at

the University of Wisconsin to determine the optical properties of these QDs and electron microscopy will be used at ORNL to determine their crystalline structure. Related theoretically issues have been addressed theoretical using density-functional approaches.

As a natural extension of the BLC idea, we have sought to find ways to achieve both spatial and size ordering without the use of an inert gas buffer layer. This effort has led to the discovery of the 2-D magic clustering approach, leading to perfectly ordered metal magic clusters on a reconstructed surface of Si(111)-(7×7).

In addition to the growth of QDs, fundamental studies have been carried out to examine the stability of QDs and nanostructures after growth. In the experimental part of this study, nanostructures of copper on Cu(100) and Cu(111) were created and then observed by scanning tunneling microscopy to see their behavior with time at room temperature. The decay behavior on the two structures was quite different with a uniform decay at all levels occurring on the Cu(111) surface, while on the Cu(100) surface, the decay occurred from the bottom of a mound first. In both cases the decay process occurred primarily through an avalanche process when one atomic height step approached a step of a supporting layer below. In the (100) case, the orientation of this supporting edge was very important, while in the (111) case, orientation was insignificant. This observation has been explained in a model study which showed that all the observed qualitative behavior could be determined by whether the system observed decayed by an any site decay mechanism or by a selective site decay mechanism.

In collaboration with Prof. Ugo Valbusa's group at the University of Genoa, Italy, we have also discovered a striking bimodal growth mode for QD formation in an entirely unexpected homoepitaxial system of Al(110), and the conceptual notions revealed in this study may significantly improve our current understanding of QD formation heteroepitaxial systems as well.

Finally, we have investigated surface intermixing of metallic alloys using first-principles density functional calculations and identified a generic rule governing the frequently observed oscillatory nature of surface alloying.

These research findings have resulted in six invited talks at major scientific meetings, including two keynote speech invitations. About 10 contributed talks have also been presented/scheduled.

Publications and Intellectual Property Derived from This Project

M. C. Chang and Z. Y. Zhang, "Self-Organized Formation of Quantum Dots Assisted by an Inert Gas Buffer Layer and Charging," *Phys. Rev. Lett*. submitted for publication (2002).

J. Shen, J. P. Pierce, G. A. Farnan, Z. Gai, A. P. Baddorf, J. F. Wendelken, E. W. Plummer, and J. Kirschner, "A Consistent Look at the World of Low-Dimensional Magnetism," *Phys. Rev. Lett*., submitted for publication (2002).

K. Varga, L. G. Wang, S. Pantelides, and Z. Y. Zhang, "Critical layer thickness in Stranski-Krastanow growth of Ge on Si(001)," *Phys. Rev. Lett*., submitted for publication (2002).

J. L. Li, Q. K. Xue, Z. Y. Zhang et al., "Spontaneous assembly of perfectly ordered identical-size nanocluster arrays," *Phys. Rev. Lett*. **88**, 066101 (2001).

M. Z. Li, J. F. Wendelken, B. G. Liu, E. G. Wang, and Z. Y. Zhang, "Decay Characteristics of Surface Mounds with Contrasting Interlayer Mass Transport Channels," *Phys. Rev. Lett.* **86**, 2345 (2001).

W. W. Pai, J. F. Wendelken, C. R. Stoldt, P. A. Thiel, J. W. Evans, and D. J. Liu, "Evolution of Two Dimensional Wormlike Nanostructures on Metal Surfaces," *Phys. Rev. Lett*. **86**, 3088 (2001).

F. Buatier de Mongeot, R. Buzio, A. Molle, C. Boragno, U. Valbusa, and Z. Y. Zhang, "Nanocrystal Formation in Al(110) Homoepitaxy: Bimodal Growth and the Role of Surface 'Kinetic Traps'," *Science*, submitted for publication (2001).

K. Varga, L. G. Wang, S. Pantelides, and Z. Y. Zhang, "Oscillatory surface intermixing in binary metallic alloys," *Phys. Rev. Lett*., submitted for publication (2002).

Z. Y. Zhang, J. F. Wendelken, M. C. Chang, and W. W. Pai, "Self-Organized Formation of Quantum Dots of a Material on a Substrate," U. S. Patent 6,313,479, November 5, 2001.

Z. Y. Zhang, J. F. Wendelken, M. C. Chang, and W. W. Pai, "Self-Organized Formation of Quantum Dots of Almost Any Material on Any Substrate," U. S. Patent application, filed March 23, 2001.

Development of High-Efficiency Solid Oxide Fuel Cell Materials

P. F. Becher,[1] C. M. Rouleau,[2] I. Kosacki,[1] T. R. Armstong,[1] D. H. Lowndes,[2] M. Z. Hu,[3] and M. Liu[4]
[1]*Metals and Ceramics Division*
[2]*Solid State Division*
[3]*Nuclear Science and Technology Division*
[4]*Georgia Institute of Technology*

This project focuses on the development of materials for the next generation of multistage solid oxide fuel cells (SOFCs) that will exhibit both exceptionally high efficiencies and fuel utilization. These fuel cells will require new oxides (e.g., electrolytes or electrodes) that can function at much lower temperatures (e.g., 500–700°C) for extended periods (40,000 h). The research focuses on the development of novel nanocrystalline and nanostructured oxides. These findings have led to the development of nanoscale highly oriented yttria-stabilized zirconia films with ionic conductivity values that exceed the highest reported values and a basis for developing multilayer films with novel conductivity behavior. Advances in chemical synthesis of nanocrystalline electrolyte films should improve the productivity and cost-effectiveness of current nanocrystalline film fabrication technology.

Zirconia electrolytes have been developed for fuel cells operating above 800°C with yttria-stabilized cubic zirconia (YSZ) offering quite acceptable ionic conductivity for these high-temperature fuel cells. However, recent studies have indicated that nanocrystalline zirconia films have the potential for far greater ionic conductivity than the conventional zirconia with micron-scale microstructures.[1] Two approaches were selected to fabricate YSZ films: pulsed laser deposition (PLD) to synthesize nanoscale thin films and a polymeric precursor (PP) coating synthesis route to produce films with nanocrystalline microstructures. The PLD process would allow highly textured (near epitaxial) growth of YSZ films to examine the effects of texture and nanoscale film thickness on the ionic conductivity. The PP coating studies focused on advances in synthesis that allow for more efficient/rapid fabrication of micron-scale coatings of nanocrystalline YSZ.

A modified PP spin-coating method was developed that can produce coatings of nanocrystalline YSZ with thicknesses of 250 to 400 nm in a single deposition, which represents an order of magnitude increases in thickness achievable per coating step. Furthermore, the nanoscale grain size of these YSZ coatings was found to be quite stable at temperatures as high as 900°C. This is a critical finding as SOFCs operate over this temperature range and retention of the nanocrystalline microstructure is critical to the cell performance.

The onset of a nanoscale effect on the ionic conductivity in PLD ZrO_2-10 mol % Y_2O_3 (10YSZ) epitaxial films was detected in films with thickness <50 nm. For example, conductivity values of 0.1 S/cm and ~0.05 S/cm are obtained at 600°C and 500°C, respectively, within a 15-nm-thick film. However, films thicker than 50 nm exhibit a temperature-dependent conductivity identical to that of bulk single crystals (e.g., 0.005 S/cm and <0.001 S/cm at 600°C and 500°C, respectively). The conductivity increased by ~140-fold in the thinnest films and does not appear to have saturated. The films, deposited on (001) MgO substrates by pulsed laser ablation, not only exhibit extremely strong cube-on-cube texture but also appear to be free of dislocations. Consequently, the observed nanoscale effect appears to be solely a function of film thickness, which suggests surface and interface conduction mechanisms dominate their behavior.

The observed exceptionally high ionic conductivity of the nanoscale YSZ films represents both a scientific breakthrough in assessing the conduction mechanisms in nanostructured oxides and a technological one for developing unique multilayer conductors and thin film sensors. This work has already attracted potential support for novel NO_x sensors from DOE Office of Transportation Technology. Two talks were presented at international meetings, and a report of possible invention and a paper were submitted on the behavior of the PLD nanoscale YSZ films.

Reference

[1]I. Kosacki, T. Suzuki, V. Petrovsky, and H. U. Anderson, *Solid State Ionics* **1225**,136–137 (2000).

Silicon Carbide Device Fabrication and Application as the Next Generation of Power Electronics

O. W. Holland,[1] L. M. Tolbert,[2] L. C. Feldman,[3] S. Islam,[2] T. J. Theiss,[4] and T. E. Haynes[1]
[1]*Solid State Division*
[2]*The University of Tennessee*
[3]*Vanderbilt University*
[4]*Engineering Science and Technology Division*

Power electronics has been identified as a cross-cutting technology vital to effective carbon management. Core competencies exist at ORNL to develop a demonstration technology—a task requiring innovations at both the device and systems level. Recent advances in materials processing and synthesis by researchers in the Solid State Division allow fabrication of SiC devices that will take full advantage of SiC's intrinsic properties. The goal of this project is to integrate SiC-based power electronics fabricated using state-of-the-art processing technology into power management modules with the goal of measurably increasing system performance.

Power electronics is severely limited by Si-based devices and requires devices capable of handling more power. The most promising candidate is SiC, a "wide bandgap" semiconductor with properties such as a large band gap, high thermal conductivity, high breakdown field strength, and high saturated drift velocity that make it suitable for applications requiring high temperature, high power, and high frequency. The large performance gains of SiC-based electronics offer benefits to many strategic industries such as electric power generation and distribution. The incorporation of solid-state "smart" power electronics into the power grid should significantly reduce the power reserve margin necessary for reliable operation. In addition, the use of SiC power electronics devices would enable more widespread use of distributed generation by providing high-power electronic interconnects to the electrical grid.

The interdisciplinary nature of this project builds upon Laboratory's strengths in materials synthesis and processing and power electronics. The key element of the project is the integration of SiC-based power electronics, fabricated using ORNL's processing technology developed into power management modules with the goal of measurably increasing the performance of such systems. Fabrication of a metal-oxide-semiconductor field-effect transistor (MOSFET), a key device for high-power switching, involves processing steps such as surface oxidation for forming a control gate and dopant implantation. The quality of the control gate determines the mobility of the conductive channel of the device in the on-state; however, problems at the oxide interface results in a low channel mobility, which significantly degrades performance in 4H-SiC MOSFETs.

We successfully developed passivation techniques using postoxidation anneals in NO and NH_3. The trap density [$D_{it}(E_c)$] at the oxide interface was found to decrease monotonically up to 1175°C. Following a 2-h anneal at 1175°C, $D_{it}(E_c)$ was reduced from ~2×10^{13} to 2×10^{12} $cm^{-2}eV^{-1}$. Modeling has shown that carbon clusters at the oxide interface are likely the cause of the poor channel mobility.

The other major processing issue involves ion implantation. Conventional processing includes high-temperature dopant implantation at >600°C. Implantation schemes, developed at ORNL, were used to fabricate metal-semiconductor field-effect transistor (MESFETs) in bulk 4H-SiC using N^+ implantation at room temperature. Measurement of channel doping showed that 50% of the implanted nitrogen was electrically active. The MESFETs operated with only a small change in DC characteristics over the temperature range of 25–350°C, indicating stable operation at high temperature as predicted.

Circuit design efforts included the development of a temperature-dependent circuit model to simulate device performance in operational circuits. Temperature profiles of devices (without heat sinking) in a motor drive of a vehicle simulated over an urban driving cycle showed that heat sink requirements for SiC devices were almost negligible. Heat sink requirements for Si devices generally make up approximately one-third of the weight and volume of the total power electronics package.

As a result of this project, DOE's Office of Advanced Automotive Technology is interested in the impact SiC can have on automotive power electronics. Also, we have been selected to submit a $3.6 million, 3-year proposal in response to the Defense Advanced Research Projects Agency call entitled "Wide Bandgap Semiconductor Technology Initiative-SOL BAA01-35."

Publication Derived from This Project

O. W. Holland et al., "A Method to Improve Activation of Implanted Dopants in SiC," *Mat. Res. Soc. Proc*. **650**, 5.3.1 (2001).

Phase Transitions and Transport in Magnetic Nanowires

J. Shen,[1] W. H. Butler,[2] T. C. Schulthess,[3] X. Zhang,[3] and U. Landmann[4]
[1]*Solid State Division*
[2]*Metals and Ceramics Division*
[3]*Computer Science and Mathematics Division*
[4]*Department of Physics, Georgia Technical University*

We have made a major breakthrough in the field of low-dimensional magnetism in the first year of this project. By using novel growth techniques, we have successfully grown two-dimensional (2-D), one-dimensional (1-D), and zero-dimensional (0-D) magnetic nanostructures consisting of *identical amounts of Fe atoms* on the same Cu(111) template. A strikingly new picture of low-dimensional magnetism has emerged from our subsequent magnetic characterizations. On the theoretical side, we have made ab initio calculations and Monte Carlo simulations on the magnetic behavior of 2-D, 1-D, and 0-D Fe on Cu(111). The combination of experimental and theoretical results is presenting an absolutely new perspective of low-dimensional magnetism. In future work we propose to extend our success on the Cu(111) template to other templates in order to obtain a better understanding of our observations. We will also extend our growth capability so that we can prepare large-area nanowire arrays for neutron and transport characterizations and, correspondingly, develop the theory of spin-dependent transport in nanowires.

A major goal in recent years has been to make magnetic and electronic devices function at ever smaller scales. In the past two decades, great success has been achieved in the study of 2-D magnetically active films, including the discovery and application of the giant magnetoresistance effect and the invention of spin-electronic devices such as spin-valve read sensors for disk drives and spin tunneling devices for non-volatile random access memory. In this project, we proposed to push this trend to its ultimate limit by investigating magnetic wires that are one to several hundred atoms in cross section. The purpose was to address fundamental questions on the existence and nature of transport and long-range magnetic order in practical realizations of 1-D systems. We undertook five major objectives chosen to address fundamental issues in the fabrication, characterization, and theory of low-dimensional magnets. In particular, we proposed to demonstrate the ability to (1) grow, in a controlled fashion, and to characterize atomic chains, stripes, and nanowires; (2) perform predictive calculations of the electronic and magnetic structure of electronic chains, stripes, and nanowires including substrate effects; (3) calculate magnetic anisotropies of chains, stripes, and nanowires; (4) grow high-quality magnetic nanowires on an insulating substrate; and (5) calculate the transport and magneto-transport properties of nanowires.

In FY 2001, we achieved the goals of controlled growth and characterization of 2-D, 1-D, and 0-D systems. In addition we made a major breakthrough in the field of low-dimensional magnetism. By using novel growth techniques, we successfully grew 2-D, 1-D, and 0-D magnetic nanostructures consisting of *identical amounts of Fe atoms* on the same Cu(111) template. As a result, a strikingly new picture of low-dimensional magnetism has emerged from our subsequent magnetic characterizations. We also successfully grew FeCo alloy wires on a W(110) substrate and Ni wires in a nanoporous template. On the theoretical side, we have made ab initio calculations and Monte Carlo simulations on the magnetic behavior of 2-D, 1-D, and 0-D Fe on Cu(111). The combination of experimental and theoretical results is presenting us an absolutely new perspective of low-dimensional magnetism.

Through this project, we are greatly enhancing our capabilities to synthesize, characterize, and calculate magnetic nanostructures at ORNL. The Fe/Cu(111) work was chosen to be presented at the 2001 DOE on-site review of ORNL, and our sponsors were quite pleased and very complimentary. We have also been invited by major conferences including American Physical Society and American Vacuum Society in 2002 to present our results. This project directly resulted in a nanomagnetism proposal that has been chosen by ORNL to bid for FY 2002–2003 DOE Nanoscale Science, Engineering, and Technology funding. The PIs are currently leading a nation-wide effort to put nanomagnetism as the research focus area in the ORNL Center for Nanophase Materials Science.

Publications Derived from This Project

J. Shen et al., "Magnetism in low dimensions: films, stripes and dots of Fe on Cu(111)," *Phys. Rev. Lett*., submitted (2002).

Z. Gai et al., "Growth of low-dimensional magnetic nanostructures on an insulator," *Appl. Phys. Lett*., submitted (2002).

M. Eisenbach et al., *Phys. Rev. B*, submitted (2002).

S.-H. Tsai et al., "Monte Carlo simulations of ordering in ferromagnetic-antiferromagnetic bilayers," *J. Appl. Phys.,* accepted for publication (2002).

G. Brown et al., "Model of Fe nanostripes on Cu(111)," *J. Appl. Phys*., accepted for publication (2002).

H. K. Lee et al., "Monte Carlo Simulations of Interacting Magnetic Nano-particles," *J. Appl. Phys*., accepted for publication (2002).

Biomolecule-Assisted Self-Assembly of Three-Dimensional Carbon Nanotube Nanostructures

M. J. Doktycz,[1] D. H. Lowndes,[2] M. L. Simpson,[3] V. I. Merkulov,[3] D. B. Geohegan,[2]
M. A. Guillorn,[3] P. F. Britt,[4] and J. Fleming[5]
[1]*Life Sciences Division*
[2]*Solid State Division*
[3]*Engineering Science and Technology Division*
[4]*Chemical Sciences Division*
[5]*The University of Tennessee*

This project addresses a critical need in molecular-scale device research: the directed self-assembly of three-dimensional (3-D) nanostructures. A novel approach that combines biological molecules with synthetic nanostructures is being pursued. We are building on previous research accomplishments and capabilities in the preparation of carbon nanotubes and deterministically grown, vertically aligned carbon nanofibers (VACNFs) to provide self-assembly in one or two dimensions. Integration in the other dimensions will come from the biomolecule-mediated assembly of single-wall carbon nanotubes (SWNTs) with other SWNTs or onto a VACNF framework. To accomplish this, we are developing the ability to combine DNA and other biomolecules with carbon nanotubes/fibers. Promising attachment and characterization techniques have been developed. We are also developing effective isolation procedures based on gel electrophoresis or column chromatography and seek to accomplish the specific self-assembly of 3-D nanostructures in the next phase of the project. This capability will enable the construction of nanoelectronic systems, biosensors, and nanomechanical devices.

This proposal specifically addresses the interface between synthetic and natural nanostructures. Our intent is to build complexes between these two materials that will enable the self-assembly of complex systems. Self-assembly exploits the physical and chemical properties of molecules to form precise ordered arrangements which are self-determined by energy minimization. Nature has developed the ability to self-assemble thousands of individual parts into precisely defined functional structures. Creating and applying a similar ability to synthetic nanostructures would enable the manufacture of intricate structures without the tedious manual construction techniques currently used. Ideally, these intricate structures could be further manipulated to self-assemble functional meso- and macro-scale objects that would be useful for applications in biomedicine, nanoelectronics, biosensors, and nanomechanical devices. However, accomplishing even the simplest self-assembly with synthetic structures represents a significant technical hurdle. Nevertheless, we believe that self-assembly could be possible with the construction of hybrid structures. These structures would combine the recognition and assembly features intrinsic to biomolecules, such as with DNA, with synthetic structures that possess useful physical properties, such as carbon nanotubes. Further, in the process of addressing self-assembly, we will develop new characterization tools and apply biomimetic solutions to various applications.

To accomplish the interfacing between biological molecules and carbon nanotubes for the eventual self-assembly of nanomaterials, the project was divided into four primary tasks: (1) the fabrication of nanotubes and ordered arrays of nanofibers, (2) the attachment of biomolecules to carbon nanotubes/nanofibers, (3) the development of nanoscale characterization techniques, and (4) the design and construction of a few example molecular assemblies. Significant progress was made in each of these areas. One key accomplishment was the demonstration of chemical and biological labeling of the carbon nanofibers. Similarly, chemical labeling of carbon nanotubes was also demonstrated. This achievement was especially challenging, as it required the simultaneous development of a chemical labeling method while developing a suitable analytical characterization technique. This accomplishment sets the stage for directed assembly of more complex structures. In addition to this accomplishment, significant progress has been made in the construction and demonstration of a biological mimic using VACNFs. Membrane structures capable of controlling particle transport have also been created and characterized.

As a result of this work, three presentations at regional and national meetings on nanotechnology have been made. Additionally, an invention disclosure has been filed as noted below.

Intellectual Property Derived from This Project

M. J. Doktycz, M. L. Simpson, D. H. Lowndes, M Guillorn, and V. I. Merkulov, "Nanoengineered Membranes for Controlled Transport," ORNL invention disclosure 1300000993, filed September 17, 2001.

Creating Oxygen-Rich Nanoclusters for High-Temperature Strengthening of Structural Alloys

D. T. Hoelzer,[1] P. J. Maziasz,[1] S. S. Babu,[1] E. A. Kenik,[1] M. K. Miller,[1] I. G. Wright,[1]
E. D. Specht,[1] J. L. Robertson,[2] and G. Sarma[3]
[1]*Metals and Ceramics Division*
[2]*Solid State Division*
[3]*Computer Science and Mathematics Division*

The proposed research will investigate a new phenomenon involving the dissolution of stable oxides and the formation of nanoscale oxygen-rich clusters that significantly enhance high-temperature strength and creep resistance of ferritic alloys. The primary focus of this project will be to develop the experimental and theoretical insights that will expand the current scientific knowledge of non-equilibrium thermodynamics, phase formation and stability, and nanoscale strengthening mechanisms at high temperatures. This understanding may also lead to new alloy design and alternative processing methods to produce a range of advanced structural alloys with superior high-temperature performance.

To meet goals for higher thermal efficiencies in energy generation systems, new advanced structural materials possessing significantly improved high-temperature, high-strength properties are required. This project addresses this need by developing the understanding of a new phenomenon involving a remarkable improvement in the high-temperature, high-strength properties of a ferritic alloy containing a dispersion of nanosize clusters of yttrium, titanium, and oxygen atoms. Our primary focus will be to investigate the evolution from mesoscale stable oxides to new nanoclusters in a ferritic alloy during mechanical alloying (MA) and the stability of nanoclusters at high temperatures. From this research project, we foresee developing the knowledge for improving the MA processing method and developing non-MA processing methods for achieving high number densities of uniformly dispersed nanoclusters.

During FY 2001, we focused on determining the stability of nanoclusters and on investigating the formation of nanoclusters in MA ferritic alloys. First, we established that nanoclusters of ~4-nm size and containing yttrium, titanium, and oxygen atoms remain very stable at high temperatures for long periods of time. Atom probe tomography showed no significant changes in size, number density, and composition of the nanoclusters, initially present in the as-processed MA Fe-12Cr-3W-0.4Ti + 0.25Y_2O_3 ferritic alloy, after being exposed to 800°C and an applied load of 138 MPa for ~14,300 h. This level of performance is several orders of magnitude better than that of any conventional Fe-Cr-based alloy. Theoretical models based on classical thermodynamics have not been able to fully account for this unexpected result showing stable nanoclusters. Second, we investigated the formation of nanoclusters in a ferritic alloy by focusing initially on nonequilibrium processing conditions leading to the instability of Y_2O_3. The effects of composition and processing were investigated by mechanically alloying pre-alloyed Fe-14Cr powders containing 3W, 0.4Ti, or 3W+0.4Ti (wt %) with 0.25% Y_2O_3 powders in a high-energy attrition mill. The high milling intensity that was used resulted in highly deformed powders containing lamellar grain structures consisting of ~10-nm-size grains and high levels of internal strains. Differences in alloy composition do not significantly affect these microstructural features. Detecting nanosize Y_2O_3 particles in the milled powders was not possible using X-ray diffraction and represented the most challenging issue for this project. However, extended X-ray absorption fine structure (EXAFS) is a promising technique that we are exploring to study changes in atomic bonding and coordination of Y_2O_3. The results from EXAFS may determine if yttrium has dissolved into the iron lattice as a result of milling; obtaining this type of result would be very beneficial to developing non-MA processing methods.

This project has opened up several promising collaborations and follow-on funding opportunities. A recent collaboration with research scientists from the French Commissariat à l'Energie Atomique (CEA) on advanced fuel and materials development with emphasis on nanocomposited steels resulted in a proposal to the International Nuclear Energy Research Initiative (I-NERI), Office of Nuclear Energy, Science and Technology, DOE. The proposed work will increase our knowledge of nanocomposited steels by focusing on the deformation and fracture modes and the effects of displacement damage on the stability of nanoclusters and oxide particles using multi-MeV heavy ions. This year we presented one invited talk and one contributed talk at international microscopy conferences and submitted one article for publication.

Nanostructured Thin-Film Super-Pockels Materials for Ultrafast Miniature Optical Switching Devices

G. E. Jellison, Jr,[1] M. L. Simpson,[2] J. T. Simpson,[2] D. B. Beach,[3] C. M. Rouleau,[1] and H. M. Christen[1]
[1]*Solid State Division*
[2]*Engineering Science and Technology Division*
[3]*Chemical Sciences Division*

One of the greatest challenges in photonics is to switch or modulate light signals using an electrical signal at ever-increasing rates. In this project, we have been studying thin films of "Super Pockels" (SP) materials, which have extremely large electro-optic (E-O) coefficients. Consequently, photonic devices made of SP materials would be considerably smaller than present $LiNbO_3$-based devices. Smaller size and larger E-O coefficients result directly in lower power devices. A second focus of our proposal was to examine photonic crystal structures in waveguides made of the SP materials. During the first year of this project, we have grown two-domain strontium barium niobate (SBN) as well as a number of other SP materials of lesser optical quality. Three diagnostic techniques are being developed that will enable ORNL to perform the measurements necessary for the characterization of these novel photonic materials.

The primary objectives of this project are film growth of E-O materials and development of appropriate optical diagnostics to characterize the resulting films.

One SP material, SBN, has been successfully grown by pulsed laser deposition on MgO using a growth chamber adapted for crossed-beam laser ablation. The initial films were optically highly absorbing (as determined by ellipsometry) and required an oxygen anneal to decrease the optical absorption. The films were epitaxial, with the c-axis perpendicular to the substrate surface, but with four growth domains, where the a-b axes were oriented at ±18.4 and at ±30.9 with respect to the (100) plane of the MgO lattice. The ±30.9 domains were eliminated when an off-cut MgO substrate [4 off the (001) toward the (100) axis] was used. This is the first study of SBN growth on off-cut MgO. Solution growth of SBN on MgO and $LaAlO_3$ was not as successful and resulted in films with some c-axis alignment, but no in-plane order. As an alternative to SBN, epitaxial growth of the bismuth-containing Aurvillius phases [such as $(Sr/Ba)Nb_2Bi_2O_9$] grown on $LaAlO_3$ has been examined. These materials are atomic-scale layers of SBN sandwiched between layers of bismuth oxide. Present samples do not have the optical quality required for waveguiding applications.

Three optical diagnostic techniques are being developed: (1) an instrument to measure very small optical retardations, (2) a Mach-Zehnder interferometer to measure very small phase changes, and (3) a prism coupler to guide visible light into waveguide structures. All of these diagnostics are essential for characterizing the E-O and light-guiding characteristics of SP thin films and further work in the area of photonics. A new configuration of two-modulator generalized ellipsometer (2-MGE) is being used to measure both the retardation and the direction of the fast optical axis as a function of position. Present resolution is ~50 μm but can be improved to ~20 μm. Measurements of a $LiNbO_3$ crystal show that the electric field is NOT uniform in the material. *No other instrument* is capable of this kind of measurement, and applications to the study of radiation detectors should prove to be interesting. The Mach-Zehnder interferometer and the prism coupler have been built but require optical-quality waveguides to be tested.

The successful completion of this project will be extremely important to the development of a potentially large portfolio of research programs in photonics at ORNL. At present, we have world-class facilities in film growth of oxide materials, as evidenced by the progress made in high-T_c superconductors. There are several patents already in place and in preparation describing PC devices that could revolutionize the use of photonics. The new Center for Nanophase Materials Science will have several facilities that can be used for either electronic or photonic applications.

Publications Derived from This Project

D. P. Hutchinson, R. K. Richards, M. L. Simpson, and J. T. Simpson, "Reflective Coherent Spatial Light Modulator," U.S. Patent, filed April 13, 2001.

New Project Abstract Project Number: 02-3211-2035

Enhanced Performance and Energy Savings Through Ultrahigh Magnetic Field Processing of Ferromagnetic Materials

G. M. Ludtka,[1] G. M. Stocks,[1] R. A. Kisner,[2] D. M. Nicholson,[3] G. Mackiewicz-Ludtka,[1]
J. B. Wilgen,[2] and J. W. Lue[4]
[1]*Metals and Ceramics Division*
[2]*Engineering Science and Technology Divison*
[3]*Computational Sciences and Engineering Division*
[4]*Fusion Energy Division*

We will develop an innovative and revolutionary processing technology that will create an entirely new research initiative for materials and materials process development within ORNL. This technology has both scientific and industrial relevance with potential annual energy savings ranging from 14 trillion BTUs for single heat-treatment applications to possible future values in excess of 1 Quad in the transportation sector through reduced gasoline usage of 10^{10} gallons per year and the accompanying significant environmental benefit of major greenhouse gas reduction. This research will demonstrate and document the influence of ultrahigh magnetic field (>5 T) processing on the phase equilibria and kinetics for a ferromagnetic material. Experiments will be conducted on the candidate material to establish the influence of ultrahigh magnetic fields. These materials will be characterized using X-ray synchrotron, neutron diffraction, and advanced microanalytical techniques to provide a fundamental understanding of the magnitude of the effects of these ultrahigh magnetic fields on the microstructures that evolve. Novel microstructures with enhanced performance are anticipated that will enable the implementation of new and lightweight materials that will lead to the major energy savings and environmental benefits for the heat treatment and transportation sectors. A parallel simulation effort using modern first-principles electronic structure methods will be conducted to calculate the contribution to the free energy of the alloy phases that results from the application of these large magnetic fields. Based on the guiding principles established by this modeling effort, new compositions with their phase equilibria will be predicted and verified experimentally. Successfully demonstrating this novel materials and process development concept, while providing a fundamental understanding and predictive capability of the potential magnitude of the effects of this ultrahigh magnetic field processing technology, will result in significant future program development and funding opportunities from several major resources. In addition, deployment of this technology will be a major step towards achieving "materials by design" goals.

New Project Abstract Project Number: 02-3211-2038

Electrical Conductivity at the Nanoscale

A. P. Baddorf,[1] C. L. Fu,[2] J. Shen,[1] H. H. Weitering,[3] J. F. Wendelken,[1] and X. Zhang[4]
[1]*Solid State Division*
[2]*Metals and Ceramics Division*
[3]*Solid State Division and The University of Tennessee*
[4]*Computer Science and Mathematics Division*

The link between the nanoscale and the human scale, be it quantum computing, nanomechanics, or nanotube devices, is almost always by electrical current. In today's world, where electronic devices proliferate, the fundamental and practical importance of understanding electronic transport in nanoscale devices is immense. This proposal focuses on measurement and calculation of conductivity in a broad class of materials with great complexity, physical richness, and promise for applications in nanotechnology, surfaces, interfaces, and ultrathin films of layered transition metal oxides (TMOs). Nanoscale TMOs are complex because the structural, electronic, and magnetic properties are strongly coupled but not always linearly. The result is ferroelectric, superconducting, and magnetoresistive

materials with great potential as optical switches, magnetic sensors, and transducers where properties can be "tuned" by the introduction of reduced dimensions, doping, or strain. Despite great interest in these materials, no studies of electron transport exist for TMOs with nanoscale dimensions.

The objective of this project is to fabricate and characterize TMOs and to make in situ measurements and calculations of electronic transport in surfaces and ultrathin films on both macroscales and nanoscales. The result will relate conductivity to structure, strain, composition, temperature, magnetism, defects, doping, and nanoscale ordering. The impact of successfully elucidating the nature of electronic transport and of learning how to engineer and control the coupled interactions in nanoscale TMOs will shift both the way we think about and the way we employ this class of materials.

New Project Abstract Project Number: 02-3211-2040

Self-Organized Copolymer and Nanoporous Oxide Thin-Film Templates for Controlled Synthesis and Periodic Replication of Nanoscale Materials

S. Dai,[1] D. B. Beach,[1] M. Dadmun,[2] D. H. Lowndes,[3] V. I. Merkulov,[4] S. J. Pennycook,[3] and C. Tsouris[5]

[1]*Chemical Sciences Division*
[2]*Department of Chemistry, The University of Tennessee*
[3]*Solid State Division*
[4]*Engineering Science and Technology Division*
[5]*Nuclear Science and Technology Division*

Two central challenges in nanoscale science and technology are, first, to develop efficient methods for synthesizing high-quality nanomaterials with well-controlled properties and, second, to direct their assembly from the nanoscale upward into functional configurations. Control of nanomaterials properties generally requires synthesis of only a narrow-size distribution, while functional assembly usually implies controlling the location and/or the orientation of the nanomaterials. It must be emphasized that the directed assembly requirement cannot be met at this time by even the highest resolution electron beam lithography (EBL), for both technical and economic reasons. Consequently, "successful" (meaning potentially useful) syntheses often will require spatially confining and directing the nanoscale growth reactions. Our recently developed nanoscale structures based on the self-assembly of surfactants or block copolymers could serve as ideal nanoreactors for efficiently synthesizing, replicating, and eventually manufacturing technologically important nanomaterials in functional configurations. The objectives of this proposal are (1) to develop new chemistry that uses self-assembly of block copolymers and interfacial reactions for formation of ordered nanoporous oxide thin films with controlled orientation and location; (2) to evolve the use of diblock coplymers as templates to design and synthesize new materials consisting of well-controlled arrays of nanostructures; (3) to develop a scientific basis that makes use of the ordered nanoporous thin films to greatly enhance selectivity in synthesis of single-walled carbon nanotubes (SWNTs) based on spatially confined growth initiated inside channels; and (4) to replicate metallic nanorods or nanowires inside the nanopore arrays of the nanostructured thin films through electroless or electrochemical deposition. The unique atomic-resolution Z-contrast microscopy at ORNL provides an essential tool to conduct detailed structural characterizations of nanomaterials. This project addresses key issues in the rational synthesis and production of highly uniform nanomaterials. The potential advantages of this approach to ORNL are truly enormous. This project will allow us to synthesize nanostructured materials that are difficult or impossible to synthesize through other technologies. Our approach, with its emphasis on using molecular self-assembly and high-yield inexpensive growth methods to produce useful quantities of true "designer nanomaterials," is a perfect candidate for new funding under nanotechnology initiatives.

Multifunctional Nanotube Composites

D. B. Geohegan,[1] P. F. Britt,[2] M. J. Lance,[3] A. A. Puretzky,[4] M. A. Guillorn,[5] S. J. Pennycook,[1]
D. A. Blom,[3] G. Pharr,[3] C. A. Blue,[3] D. C. Joy,[3] and M. H. McCay[6]

[1]*Solid State Division*
[2]*Chemical Sciences Division*
[3]*Metals and Ceramics Division*
[4]*Solid State Division and the Materials Science and Engineering Department, The University of Tennessee*
[5]*Engineering Science and Technology Division*
[6]*Center for Laser Applications, The University of Tennessee Space Institute*

Nanocomposites utilizing the great axial strength (>1 TPa) of single-wall carbon nanotubes (SWNTs) are envisioned as the ultimate structural materials. SWNTs in single crystals, fibers, or as structural reinforcing agents in softer materials, such as organic polymers, are predicted to form strong, lightweight composites far superior to those used today in aerospace, transportation, and commercial products. In addition to light weight and great strength, the sensitive coupling between electrical, mechanical, and thermal properties in SWNTs is envisioned to bring additional functionality to SWNT nanocomposites, such as actuation, directional heat transfer, gas storage, sensing, or tunable optical properties. This project aims to develop Laboratory capabilities in the synthesis and characterization of multifunctional nanocomposites using nanotubes. The project addresses the need for coordinating materials science, chemistry, and characterizational tools for the development of strong, multifunctional nanocomposites.

Central to the project is control over the chemical bonding at the interface between the nanotubes and the matrix, which determines the strength of the composite. Nanotube/polymer chemistry will be developed in concert with novel processing methods to disperse and align SWNTs in polymers for strong, functional bulk materials and fibers. The direct growth of interwoven SWNT in carbonaceous matrices will also be explored for single-step SWNT-carbon composite formation, exploiting recent discoveries at ORNL that SWNTs can be grown through simple annealing treatments. “Nanowelding” carbon nanotubes will be explored to increase the strength and modify the properties of the composites. In addition to developing microscopy and electrical measurement techniques, this project will also develop tools to characterize and relate nanostructure, interfacial binding, and mechanical properties in the nanocomposites, including in situ field emission scanning electron microscopy and micro-Raman spectroscopy during stress-strain measurements, atomic force microscopy–nanoindentation and scratching techniques, and nanoprobing by electron energy loss spectroscopy.

Multiscale Modeling and Simulation of the Growth and Functionalization of Nanotube Crystals, Arrays, and Polymeric Composites

R. F. Wood,[1] D. W. Noid,[2] S. Pannala,[2] B. G. Sumpter,[2] J. C. Wells,[2] and Z. Y. Zhang[1]
[1]*Solid State Division*
[2]*Computer Science and Mathematics Division*

The inherent complexity and diversity of most nanosystems provide compelling reasons for utilizing the full power of contemporary computational materials science to complement and guide experimental research. The situation in carbon nanotube research is particularly urgent. Nobel laureate Richard Smalley has emphasized repeatedly his view that carbon nanotube–based technology will soon rival present-day silicon technology and even supplant it in many areas. Yet it remains true that the role of the metal catalytic particles in nucleating and controlling the growth of nanotubes is entirely unresolved. With this in mind, and stimulated by ongoing experimental and theoretical work at ORNL, we propose to develop and apply a suite of advanced computational techniques and computer programs to simulate the growth and physical properties of nanotube crystals, nanofiber arrays, and polemeric composites containing them. Specific issues that will be addressed are (1) fundamental atomic and mesoscopic mechanisms in the growth of carbon nanotube crystals and nanofiber arrays, (2) simulation of composites of nanotubes and polymers and an understanding of the origins of their physical properties, and (3) chemical decoration and cross-linking of tubes and fibers to functionalize them for specific applications. The computational techniques will span multiple time and space domains and use continuum heat transfer, first-principle electronic structure, molecular dynamics, and molecular mechanics calculations. The research will be closely coordinated with related experimental programs at ORNL, and a synergism to strengthen both the computational and experimental research in the nanoscience area will be a prime objective.